

# MODELING AND SIMULATION OF WAVEFORM CHANNELS

### 14.1 Introduction

Modern communication systems operate over a broad range of communication channels including twisted pairs of wires, coaxial cable, optical fibers, and wireless channels. All practical channels introduce some distortion, noise, and interference. Appropriate modulation, coding, and other signal-processing functions such as equalization, are used to mitigate the degradation induced by the channel and to produce a system that satisfies the throughput and quality of service objectives while meeting the constraints on power, bandwidth, complexity, and cost. If the channel is relatively benign (e.g., does not significantly degrade the signal), or is well characterized, the design of the communication system is relatively straightforward.

What complicates the design is that many communication channels, such as the mobile radio channel, introduce significant levels of interference, distortion, and noise. The mobile radio channel is also time varying and undergoes fading. In addition, some channels are so variable that they are difficult to characterize. Furthermore, wireless communication systems, such as next-generation PCS, must be designed to operate over radio channels all over the world, in a variety of envi-

ronments from urban areas to hilly terrains, and under a wide variety of weather conditions. While it is possible to build prototypes of a proposed system and field-test the prototype in many locations around the globe, such an approach will be very expensive and will not be feasible in the early stages of the system design process when a number of candidate designs must be explored. The only feasible approach is to create appropriate models for the channel, and base the *initial design* on those models.

Given either deterministic or statistical models for communications channels, it might be possible, at least in the initial stages of communication system design, to use analytical approaches for evaluating the performance of a given design. For example, if we can assume that the “fading” in a channel has a Rayleigh amplitude probability density function, and the noise is additive Gaussian, the probability of error for a binary communication system operating over this channel can be expressed as

$$P_e = 1/2\bar{\gamma}_b \quad (14.1)$$

where  $\bar{\gamma}_b$  is the “average” value of the signal-to-noise ratio (SNR) at the receiver input. This expression can then be used to determine such things as the transmitter power required to ensure a given error probability. However, when the system is actually built, implementation effects such as nonideal filters and nonlinear amplifiers must be considered. These effects are difficult to characterize analytically and, in most cases, one must resort to simulation or to a combination of simulation and analytical analysis. Thus, modeling and simulation play a central role in the design of communication systems. These two topics are covered in this chapter with an emphasis on simulation approaches and methodologies for wireless communication channels.

### 14.1.1 Models of Communication Channels

While a communication channel represents a physical medium between the transmitter and the receiver, the “channel model” is a representation of the input-output relationship of the channel in mathematical or algorithmic form. This model may be derived from measurements, or based on the theory of the physical propagation phenomena. Measurement-based models lead to an empirical characterization of the channel in the time or frequency domain, and often involve statistical descriptions in the form of random variables or random processes. The parameters of the underlying distributions and power spectral densities are usually estimated from measured data. While measurement-based models instill a high degree of confidence in their validity, and are often the most useful models for successful design, the resulting empirical models often prove unwieldy and difficult to generalize unless extensive measurements are collected over the appropriate environments. For example, it is very difficult to use measurements taken in one urban location to characterize a model for another urban location unless a substantial amount of data is collected over a wide variety of urban locations, and the necessary underlying theory is available to justify extrapolating the model to the new location.

Developing mathematical models for the propagation of signals over a transmission medium requires a good understanding of the underlying physical phenomena. For example, to develop a model for an ionospheric radio channel, one must understand the physics of radio-wave propagation. Similarly, a fundamental understanding of optical sciences is needed to develop models for single mode and multimode optical fibers. Communication engineers rely on experts in the physical sciences to provide the fundamental models for different types of physical channels.

One of the challenges in channel modeling is the translation of a detailed physical propagation model into a form that is suitable for simulation. Mathematical models, from a physical perspective, might often be extremely detailed and may not be in a form suitable for simulation. For example, the mathematical model for a radio channel may take the form of Maxwell's equations. While accurate, this model must be simplified and converted to a convenient form, such as a transfer function or impulse response, prior to using it for simulation. Fortunately, this is a somewhat easier process than deriving fundamental physical models and specifying the parameters of such models. Once a physical model has been derived, and the parameter values specified, translating the physical model into a simulation model (algorithm) is usually straightforward.

### 14.1.2 Simulation of Communication Channels

Physical communication channels such as wires, wave guides, free space, and optical fibers often behave linearly. Some channels, such as the mobile radio channel, while linear, may behave in a random time-varying manner. The simulation model of these channels falls into one of the following two categories:

1. Transfer function models for time-invariant channels. Examples are wires, free-space propagation, and optical fibers. In such models, the channel is assumed to be static in nature (i.e., the channel has a time-invariant impulse response), which provides a particular frequency response due to the fixed delays within the channel. The transfer function of the time-invariant channel is said to be “flat” if the applied message source has a bandwidth for which the channel has a constant gain response. The channel is said to be “frequency selective” if the applied modulated message source has a bandwidth over which the channel has a significant gain variation.
2. Tapped delay line (TDL) models for time-varying channels. An important example is the mobile radio channel. For these channel models, the channel is assumed to vary over time. If the channel changes during the smallest time interval of interest for an applied signal, the channel is said to be “fast fading.” If the channel remains static for a large number of consecutive symbols of the applied source, the channel is said to be “slow fading” and the channel can be treated as in (1) above over the particular span of time for which the channel is static.

Transfer function models can be simulated in either the time domain or frequency domain using finite impulse response (FIR) or infinite impulse response (IIR) filters.

Empirical models in the form of measured or synthesized impulse or frequency responses are usually simulated using FIR techniques. Analytical expressions for the transfer function are easier to simulate using IIR techniques. IIR and FIR filters were discussed in detail in Chapter 5.

Simulation models for randomly time-varying (fading) channels take the form of TDLs with tap gains and delays that are random processes. Given the random process model for the underlying time variations (fading), the properties of the tap gain process can be derived and simulated using the techniques discussed in Chapter 13. If the channel is assumed to be slowly time varying, so that channel conditions do not change over many transmitted symbols, then we can use a snapshot (i.e., static impulse response) of the channel for simulation. This may be repeated as channel conditions change. By repeating the simulations for a large number of channel conditions, we can infer system performance over longer periods of time using performance measures, such as outage probabilities, as discussed in Chapter 11.

### 14.1.3 Discrete Channel Models

The focus of this chapter is on waveform-level channel models, which are used to represent the physical interactions between a transmitted waveform and the channel. Waveform channel models are sampled at an appropriate sampling frequency. The resulting samples are processed through the simulation model. Another technique, which is often more efficient for some applications, is to represent the channel by a finite number of states. As time evolves, the channel state changes in accordance with a set of transition probabilities. The channel can then be defined by a Markov chain. The resulting channel model most often takes the form of a hidden Markov model (HMM). Assuming that the HMM is constructed correctly, simulations based on the HMM allow the performance of a communication system to be accurately characterized with minimum computational burden. Discrete channel models and HMMs are the subject of the following chapter.

### 14.1.4 Methodology for Simulating Communication System Performance

Simulating the performance of a communication system operating over a time-invariant (fixed) channel is rather straightforward. The channel is simply treated as another linear time-invariant (LTIV) block in the system. Time-varying channels, on the other hand, require a number of special considerations. The methodology used will depend on the objective of the simulation and whether the channel is varying slowly or rapidly with respect to the signals and subsystems that are being simulated. Another important factor is the relationship between the bandwidth of the applied signal and the bandwidth of the channel. The complexity of a useful channel model is a function of both the time and frequency characteristics of both the source and the channel.

### 14.1.5 Outline of Chapter

The first part of this chapter is devoted to the development of models for communication channels, starting with simple transfer function models for “wired” or “guided” channels. These channels include twisted pairs, cables, waveguides, and optical fibers. These channels are linear and time invariant and, therefore, a transfer function or static impulse response model is sufficient. We then consider models for free space radio channels that are linear but may be time varying.

The second part of this chapter deals with the simulation of communication channels with the emphasis on the implementation of TDL (tapped delay line) models for randomly time-varying channels. Three different TDL models of increasing complexity and capabilities are developed.

We conclude the chapter with the description of a methodology for simulating the performance of communication systems operating over fading channels. Throughout the chapter, near-earth and mobile communication channels will be emphasized, since these channels present most of the challenges in the modeling and simulation of channels, and also because of the current high level of interest in wireless communications.

## 14.2 Wired and Guided Wave Channels

Electrical communication systems use a variety of conducting media such as twisted pairs of wires and coaxial cable. These channels can be adequately characterized by RLC circuit models, and the input-output signal transfer characteristics can be modeled by a transfer function. Cable manufacturers often provide impedance characteristics of the transmission line models for the cables, and it is easy to derive transfer function models from this data. The transfer function is then used as a simulation model. It is also easy to measure the frequency response of varying lengths of cable and derive a transfer function model based on the resulting measurements. In a large cable network it might be necessary to define the channel using a number of random variables that characterize the parameters of a resulting transfer function or static impulse response. The channel, in that instance, may be treated as time invariant and, therefore, a time-varying model is not needed.

Waveguides and optical fibers can also be included in the broad category of guided wave transmission media. While the mode of propagation might vary, channels in this category can be modeled as time-invariant linear systems characterized by transfer functions.

Guided lightwave communication systems use optical fibers, while free-space optical communication systems transmit light through the air. The most common type of lightwave communication system uses either a single-mode or multimode fiber cable as the channel, and has a binary digital source and a receiver that makes a decision based on the energy received during each bit interval.

Besides attenuating the transmitted pulses, the optical fiber distorts or spreads the transmitted pulses. There are two different distortion mechanisms: chromatic dispersion and intermodal dispersion. Chromatic dispersion is a result of the differences in the propagation velocities of different transmitted spectral components.

Intermodal dispersion is seen in multimode fibers and results from a large number of propagation paths traveling along the fiber and arriving at the detector input with different delays. This is a multipath effect. Joints and splices in a fiber network cause reflections that can be approximated as additional intermodal dispersion. The multipath channel model was briefly introduced in Chapter 4 and will be studied in more detail in Section 14.4. While the emphasis in Section 14.4 is on the fading radio channel, the material to be presented is applicable to a wide variety of channels, including cables and optical fibers.

The relationship between the input and the output of a fiber can be described by the lowpass equivalent transfer function [1, 2]

$$H(f) = \int_{-\infty}^{\infty} S(\lambda)G(\lambda)H_{im}(\lambda)H_c(\lambda, f)d\lambda \quad (14.2)$$

where  $S(\lambda)$  is the source spectrum as a function of wavelength  $\lambda$ ,  $G(\lambda)$  is the frequency-selective gain of the fiber,  $H_{im}(\lambda)$  is the intermodal dispersion, and  $H_c(\lambda, f)$  is the chromatic dispersion [2]. The intermodal dispersion is

$$H_{im}(f) = \frac{1}{\sigma_{im}\sqrt{2\pi}} \exp \left[ (-\sigma_{im}^2(2\pi f)^2/2) - j2\pi f t_d \right] \quad (14.3)$$

where  $\sigma_{im}$  is the rms impulse response width and  $t_d$  is the fiber time delay. The chromatic dispersion is

$$H_c(\lambda, f) = \exp[-j2\pi f l T(\lambda)] \quad (14.4)$$

where  $l$  is the fiber length and  $T(\lambda)$  is the group delay of the fiber [2].

The source spectrum  $S(\lambda)$ , the dispersion characteristics  $T(\lambda)$ , and the loss  $L(\lambda)$  are obtained from the manufacturer's data sheets for the source and the fiber, and are used to compute the transfer function by substituting them in (14.2) and carrying out the integration numerically for different values of  $f$ . Several approximations for  $S(\lambda)$  and  $T(\lambda)$  are used to simplify the computation of the transfer function [1, 2, 3]. For example, the source spectrum can be assumed to be a frequency impulse for ideal sources. A Gaussian approximation with mean  $\lambda_0$  can be used for most practical sources. The group delay function is often approximated by a parabolic function in  $\lambda - \lambda_0$ . Once the integral in (14.2) is evaluated, it is stored in tabular form, and the simulations are carried out using an FIR implementation for the channel.

The model given in (14.2) is an input power to output power transfer function model for the fiber, and is valid for use in direct detection lightwave communication systems in which the source spectrum is very narrow compared to the modulation bandwidth. For wideband systems, and for coherent optical communication systems, the model is not valid. The reader is referred to the lightwave communications literature for appropriate transfer function models for these systems [1, 2, 3].

### 14.3 Radio Channels

Radio channels have been used for long-distance communications since the early days of electrical communications starting with Marconi's experiments in radio

telegraphy. The propagation of radio waves through the atmosphere, including the ionosphere, which extends several hundred kilometers above the surface of the earth, is an extremely complex phenomenon. Atmospheric propagation takes on a wide range of behaviors depending on many factors including the frequency and bandwidth of the signal, the types of antennas used, the terrain between the transmit and receive antennas (rural, urban, indoor, outdoor, etc.), and weather conditions (clear air, rain, fog, etc.). Atmospheric scientists have devoted considerable effort to the understanding and development of models that describe radio-wave propagation through the atmosphere. Also, many measurement programs were carried out over the past several decades to gather empirical propagation data for HF to microwave. All of these efforts have led to a somewhat better understanding of how to model radio-wave propagation through the atmosphere, and how to use these models to aid in the analysis, design, and simulation of modern communication systems. The literature on modeling radio channels is vast and any effort to summarize this literature in a few pages would be inadequate. Nevertheless, we will attempt to provide the reader with a sampling of the various approaches to modeling and simulating communication systems.

From a communication systems designer's point of view, propagation models fall into two categories: those that aid in the calculation of path losses and those that aid in the modeling of signal distortion that may be due to multipath effects or random variations in the propagation characteristics of the channel. While the first category of models is used to establish the link power budgets and coverage analysis during initial design, it is the latter class of models that aid in the detailed design of communication systems. Hence, our focus will be on the second category of models, with an emphasis on approaches to simulating them efficiently.

We begin our discussion of channel models with an "almost" free-space channel that treats the region between the transmit and receive antennas as being free of all objects that might absorb or reflect RF energy. It is also assumed that the atmosphere behaves as a uniform and nonabsorbing medium, and that the earth is infinitely far away from the propagation path. Such a model is, for example, appropriate for satellite links.

In this idealized model, the channel simply attenuates the signal, and waveform distortion does not occur. The attenuation is computed according to the *free-space propagation model* defined by

$$L_f = \left( \frac{4\pi d}{\lambda} \right)^2 \quad (14.5)$$

where  $\lambda$  is the wavelength of the transmitted signal and  $d$  is the distance between the transmitter and receiving antennas, both of which are assumed to be omnidirectional. The transmitter and receiver antenna gains are taken into account while calculating the actual received power.

For most practical channels in which the signal propagates through the atmosphere and near the ground, the free-space propagation channel assumption is not adequate. The first effect that must be included is the atmosphere, which causes absorption, refraction, and scattering. Absorption due to the atmosphere,

when considered over narrow bandwidths, results in additional attenuation. However, over larger bandwidths, absorption is frequency dependent and can usually be modeled by a transfer function. This filtering effect can be considered time invariant, or at least quasi-static, since the channel is very slowly changing with respect to the signal. Other atmospheric phenomena, such as phase distortion introduced by the ionosphere, can also be modeled by a phase response that is slowly varying or time invariant. Several examples of transfer function models used to characterize certain types of atmospheric channels are described in the following paragraphs.

Other atmospheric effects (other than absorption) and the presence of ground and other objects near the transmission path often lead to what is known as multipath propagation. Multipath propagation is the arrival of a signal over multiple reflected and/or refracted paths from the transmitter to the receiver. These effects can also be time varying due to changes in atmospheric conditions or relative motion of the transmitting and receiving antennas, as is the case in mobile communications. The term *scintillation*, which originated in radio astronomy, is used to describe time variations in channel characteristics due to physical changes in the propagation medium, such as variations in the density of ions in the ionosphere that reflect high frequency (HF or shortwave) radio waves. Multipath fading is the terminology used in mobile communications to describe changes in channel conditions and the resulting changes in the received signal characteristics. Models for multipath fading channels will be covered in a later section of this chapter.

### 14.3.1 Tropospheric Channel

Tropospheric (non-ionospheric) communications use VHF (30 to 300 MHz) and UHF (300 MHz to 3 GHz) frequency bands for communications over distances up to several hundred kilometers. In these frequency bands, the oxygen and water vapor present in the atmosphere absorb RF energy. The loss due to absorption is dependent on the frequency of the RF wave as well as the atmospheric conditions, particularly the relative humidity. A typical set of characteristics for propagation losses due to atmospheric absorption is given in [4].

The frequency selective absorption characteristics of the atmosphere can be approximated by a transfer function of the form [4]

$$H(f) = H_0 \exp\{j0.02096f [10^6 + N(f)] l\} \quad (14.6)$$

where  $N(f)$  is the complex refractivity of the atmosphere in parts per million, and is given by

$$N(f) = N_0 + D(f) + jN''(f) \quad (14.7)$$

In (14.6) and (14.7)  $H_0$  is a constant,  $N_0$  is the frequency dependent refractivity,  $D(f)$  is the refractive absorption,  $N''(f)$  is the absorption, and  $l$  is the distance in km. These parameters are dependent on frequency and atmospheric conditions such as temperature, barometric pressure, and relative humidity. Typical values are tabulated in [4].

Given the atmospheric conditions and the bandwidth occupied by the transmitted signal, the transfer function can be computed empirically for various values of frequency using (14.6) and (14.7). The lowpass equivalent transfer function can be obtained by frequency translation, and the resulting channel model can be simulated using FIR techniques.

### 14.3.2 Rain Effects on Radio Channels

Rain has a significant impact on microwave propagation at higher frequencies (greater than 10 GHz), since the size of the rain drops is on the order of the wavelength of the transmitted signal. Various techniques have been proposed in the literature for modeling the effects of rain [5, 6]. The attenuation due to rainfall is a function of the rate of rainfall and frequency. At higher frequencies and rain rate, rain-induced attenuation, as well as depolarization, is much more significant. Thus, attenuation increases as both rain rate and frequency increase. In addition, there are resonant peaks in the attenuation characteristic that result in significantly greater attenuation in the neighborhood of these peaks. Substantial resonant peaks occur at 22 GHz and 60 GHz. The peak at 22 GHz is due to water vapor, and the peak at 60 GHz is due to molecular oxygen. These effects are well documented [5].

Attenuation curves due to rainfall are usually computed for a given geographic location using the statistics of the rain rates for that location. For satellite communications, the attenuation is computed as a function of the elevation angle of the ground station antenna (with respect to the horizon) and frequency. Lower elevation means that there is more rain water in the transmission path and hence the attenuation is higher. The effect of rainfall is typically computed for a given outage probability, which is the fraction of the time that the link BER will exceed an acceptable threshold value (usually  $10^{-3}$  for voice communications and  $10^{-6}$  for data links).

Over relatively small bandwidths, the effects of rain can be accounted for by simply including an additional attenuation term in the channel model. However, as the bandwidth of the signal becomes larger, the attenuation varies over the bandwidth, and a transfer function type model is required. The amplitude response of the transfer function has a linear tilt [on a log (dB) scale] and the phase can be assumed linear.

Free-space propagation channels at higher frequencies generally use highly directional antennas that have a particular polarization characteristic. When the carrier frequency is such that the wavelength is much greater than the size of atmospheric particles, and when there are no physical obstructions to induce multipath, it becomes possible to use antenna polarization to isolate channels. In communication systems that use multiple orthogonal polarizations for different signals, the depolarizing effect of rain must be considered. Depolarization means that energy in one polarization leaks into, or couples with, the energy in the orthogonal polarization. This produces cross-talk [6, 7, 8]. If the two signals that are transmitted on orthogonal polarizations are

$$\tilde{s}_i(t) = A_i(t) \exp [j\phi_i(t)], \quad i = 1, 2 \quad (14.8)$$

the simplest model for the two received signals with depolarization is

$$\begin{aligned}\tilde{r}_1(t) &= \alpha_{11}\tilde{s}_1(t) + \alpha_{12}\tilde{s}_2(t) \\ \tilde{r}_2(t) &= \alpha_{21}\tilde{s}_1(t) + \alpha_{22}\tilde{s}_2(t)\end{aligned}\tag{14.9}$$

where the ratio  $20 \log(\alpha_{11}/\alpha_{21})$  is a measure of the cross-polarization interference (or XPI) on signal 1 from signal 2. While a variety of approximations are available in the literature for analyzing the effects of XPI on analog and digital communication systems, the need for simulation increases as the system departs from the ideal.

## 14.4 Multipath Fading Channels

### 14.4.1 Introduction

We now turn our attention to the modeling and simulation of multipath and motion-induced fading, which are two of the most severe performance-limiting phenomena that occur in wireless radio channels. In any wireless communication channel there can be more than one path in which the signal can travel between the transmitter and receiver antennas. The presence of multiple paths may be due to atmospheric reflection or refraction, or reflections from buildings and other objects. Multipath and/or fading may occur in all radio communication systems. These effects were first observed and analyzed for HF troposcatter systems in the 1950s and 1960s [9]. Much of the current interest is in the modeling and simulation of multipath fading in mobile and indoor wireless communications in the 1 – 60 GHz frequency range. Although the fading mechanisms may be different, the concepts of modeling, analysis, and simulation are the same.

### 14.4.2 Example of a Multipath Fading Channel

To illustrate the basic approach to modeling fading channels, let us consider a mobile communication channel in which there are two distinct paths (or rays) from the mobile unit to a fixed base station, as illustrated in Figure 14.1. Although Figure 14.1 shows only two paths, it is easily generalized to  $N$  paths. For the  $N$ -path case the channel output (the input signal to the mobile receiver) is

$$y(t) = \sum_{n=1}^N a_n(t)x(t - \tau_n(t))\tag{14.10}$$

where  $a_n(t)$  and  $\tau_n(t)$  represent the attenuation and the propagation delay associated with the  $n^{\text{th}}$  multipath component, respectively. Note that the delays and attenuations are shown as functions of time to indicate that, as the automobile moves, the attenuations and delays, as well as the number of multipath components, generally change as a function of time. In (14.10) the additional multipath components are assumed to be caused by reflections from both natural features, such as mountains, and manmade features, such as additional buildings. Furthermore, each multipath component or ray may be subjected to local scattering in the vicinity of the mobile due the presence of objects such as signs, road surfaces,

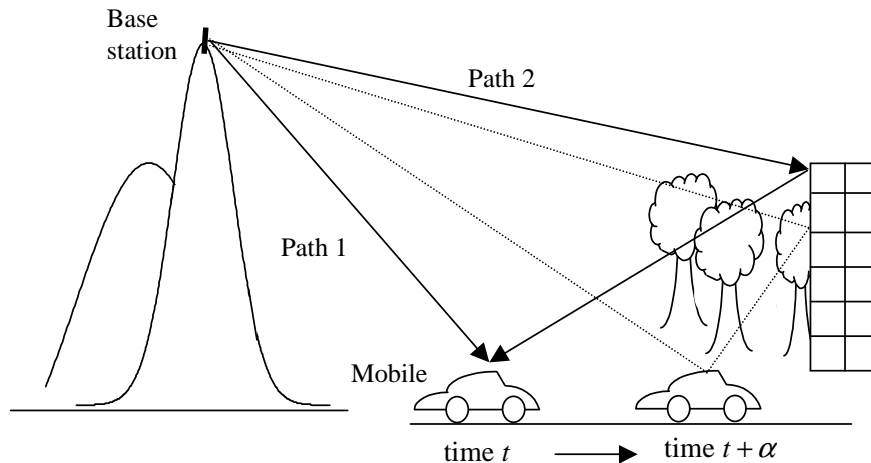


**Figure 14.1** Example of a multipath fading channel.

Source: M. C. Jeruchim, P. Balaban, and K. S. Shanmugan, *Simulation of Communications Systems*, 2nd ed., New York: Kluwer Academic/Plenum Publishers, 2000.

and trees located near the mobile. The total signal that arrives at the receiver is made up of the sum of a large number of scattered components. These components add vectorially with random phases and hence the resulting complex envelope can be modeled as a complex Gaussian process by virtue of the central limit theorem. Movement over small distances of the order of  $\lambda/2$  (about 15 cm at 1 GHz) can result in significant phase changes in the scattered components within a ray and cause components that add constructively at one location to add destructively at a location just a short distance away. This results in rapid fluctuations in the received signal amplitude/power and this phenomenon is called small scale or fast fading.

It should be noted that the small-scale fading is caused by changes in phase rather than by path attenuation, since the path lengths change by only a small amount over small distances. On the other hand, if the mobile moves over a larger distance and the path length increases from 1 km to 2 km, the received signal strength will drop, since the attenuation will change significantly. Movement over larger distances ( $\gg \lambda$ ) and changes in terrain features affect attenuation and received signal power slowly. This phenomenon is called large-scale or slow fading and is modeled separately as discussed in the following sections of this chapter.

We have seen that the complex envelope of the receiver input due to a large number of scattered components is a complex Gaussian process. For the case in which this process is zero mean, the magnitude of the process is Rayleigh. If a line-of-sight (LOS) component is present, the process becomes Ricean. The effect of this will be demonstrated in Example 14.1.

The definition of fast fading and slow fading are, to some extent, in the eye of the beholder. However, when speaking about fast and slow fading we usually have an underlying symbol rate in mind. Slow-fading channels are typically defined as channels in which the received signal level is essentially constant over many symbols or data frames. Fast fading typically means that the received signal strength changes significantly over time intervals on the order of a symbol time. The definition of fast fading and slow fading therefore depends upon the underlying symbol rate.

We now determine the complex envelope of the received signal. Assume that the channel input (the transmitted signal) is a modulated signal of the form

$$x(t) = A(t) \cos(2\pi f_c t + \phi(t)) \quad (14.11)$$

Since waveform simulation is usually accomplished using complex envelope signals, we now determine the complex envelope for both  $x(t)$  and  $y(t)$ .

The complex envelope of the transmitted signal is, by inspection,

$$\tilde{x}(t) = A(t) \exp[\phi(t)] \quad (14.12)$$

Substituting (14.11) for  $x(t)$  in (14.10) gives

$$y(t) = \sum_{n=1}^N a_n(t) A(t - \tau_n(t)) \cos[2\pi f_c(t - \tau_n(t)) + \phi(t - \tau_n(t))] \quad (14.13)$$

which can be written

$$y(t) = \sum_{n=1}^N a_n(t) A(t - \tau_n(t)) \cdot \operatorname{Re} \left\{ \exp[j\phi(t - \tau_n(t))] \exp[-j2\pi f_c \tau_n(t)] \exp(j2\pi f_c t) \right\} \quad (14.14)$$

Since  $a_n(t)$  and  $A(t)$  are both real, (14.14) can be written

$$y(t) = \operatorname{Re} \left\{ \sum_{n=1}^N a_n(t) A(t - \tau_n(t)) \exp[j\phi(t - \tau_n(t))] \cdot \exp[-j2\pi f_c \tau_n(t)] \exp(j2\pi f_c t) \right\} \quad (14.15)$$

From (14.12) we recognize that

$$A(t - \tau_n(t)) \exp[j\phi(t - \tau_n(t))] = \tilde{x}(t - \tau_n(t)) \quad (14.16)$$

so that

$$y(t) = \operatorname{Re} \left\{ \sum_{n=1}^N a_n(t) \tilde{x}(t - \tau_n(t)) \exp[-j2\pi f_c \tau_n(t)] \exp(j2\pi f_c t) \right\} \quad (14.17)$$

The complex path attenuation is defined as

$$\tilde{a}_n(t) = a_n(t) \exp[-j2\pi f_c \tau_n(t)] \quad (14.18)$$

so that

$$y(t) = \operatorname{Re} \left\{ \sum_{n=1}^N \tilde{a}_n(t) \tilde{x}(t - \tau_n(t)) \exp(j2\pi f_c t) \right\} \quad (14.19)$$

Thus, the complex envelope of the receiver input is

$$\tilde{y}(t) = \sum_{n=1}^N \tilde{a}_n(t) \tilde{x}(t - \tau_n(t)) \quad (14.20)$$

The channel input-output relationship defined by (14.20) corresponds to a linear time-varying (LTV) system with an impulse response

$$\tilde{h}(\tau, t) = \sum_{n=1}^N \tilde{a}_n(t) \delta(t - \tau_n(t)) \quad (14.21)$$

In (14.21),  $\tilde{h}(t, \tau)$  is the impulse response of the channel measured at time  $t$  assuming that the impulse is applied at time  $t - \tau$ . Thus,  $\tau$  represents the *elapsed time* or the propagation delay. In the absence of movement or other changes in the transmission medium, the input-output relationship is time invariant even though multipath is present. In this case, the transmission delay associated with the  $n^{\text{th}}$  propagation path and the path attenuation are constant (the channel is fixed) and

$$\tilde{y}(t) = \sum_{n=1}^N \tilde{a}_n \tilde{x}(t - \tau_n) \quad (14.22)$$

For the fixed-channel case, the channel can be represented in the time domain by an impulse response of the form

$$\tilde{h}(\tau) = \sum_{n=1}^N \tilde{a}_n \delta(\tau - \tau_n) \quad (14.23)$$

The corresponding representation in the frequency domain is

$$H(f) = \sum_{n=1}^N \tilde{a}_n \exp(-j2\pi f \tau_n) \quad (14.24)$$

We see that for the time-invariant channel case, the channel simply acts as a filter on the transmitted signal.

**Example 14.1.** In this example we simulate the BER performance of a QPSK system operating over a fixed 3-ray multipath channel with AWGN, and compare the BER performance with an identical system operating over an ideal AWGN channel (no multipath). In order to simplify the simulation model we will make the following assumptions:

1. The channel has three paths consisting of an unfaded LOS path and two Rayleigh components. The received power levels associated with each path, and the differential delays between the three paths, are simulation parameters.
2. The Rayleigh fading in the channel affects only the amplitude of the transmitted signal. The instantaneous phase is not affected.
3. The magnitude of the attenuation of each multipath component is constant over a symbol interval and has independent values over adjacent intervals (no doppler spectral shaping required).
4. No transmitter filtering is used, and the receiver model is an ideal integrate-and-dump receiver.

The received signal for this example can be written as

$$\tilde{y}(t) = \underbrace{a_0 \tilde{x}(t)}_{\text{LOS}} + \underbrace{a_1 R_1 \tilde{x}(t)}_{\text{Rayleigh}} + \underbrace{a_2 R_2 \tilde{x}(t - \tau)}_{\text{Delayed Rayleigh}} \quad (14.25)$$

where  $R_1$  and  $R_2$  are two independent Rayleigh random variables representing the attenuation of the two Rayleigh paths, and  $\tau$  is the relative delay between the two Rayleigh components. The Fourier transform of (14.25) is

$$\tilde{Y}(f) = a_0 \tilde{X}(f) + a_1 R_1 \tilde{X}(f) + a_2 R_2 \tilde{X}(f) \exp(-j2\pi f \tau) \quad (14.26)$$

which leads to the channel transfer function

$$\tilde{H}(f) = a_0 + a_1 R_1 + a_2 R_2 \exp(-j2\pi f \tau) \quad (14.27)$$

Clearly, if the product  $f\tau$  is not negligible over the range of frequencies occupied by the signal, the channel is frequency selective, which leads to delay spread and ISI. The values of  $a_0$ ,  $a_1$ , and  $a_2$  determine the relative power levels  $P_0$ ,  $P_1$ , and  $P_2$  of the three multipath components.

Simulations were conducted for each of the six sets of parameter values given in Table 14.1. For each scenario, the BER is evaluated using semianalytic estimation. In Table 14.1, the delay is expressed in terms of the sampling period. Since the simulation sampling frequency is 16 samples per symbol,  $\tau = 8$  corresponds to a delay of one-half the sample period. (See Appendix for code.)

The simulation results for Scenarios 1 and 2 are illustrated in Figure 14.2. In Scenario 1, only a line-of-sight component is present. There is no multipath for Scenario 1 and this result provides the semianalytic estimation of the BER for a QPSK system operating in an AWGN environment. This simulation serves to verify the simulation methodology and provide baseline results representing an ideal QPSK system. For comparison purposes, this result is displayed along with the BER results for all five of the remaining scenarios. Table 14.1 shows that Scenario 2 results by adding a Rayleigh fading component to the LOS component of Scenario 1. This gives rise to a Ricean fading channel. Since  $\tau = 0$ , Scenario 2 is flat fading (not

Table 14.1 Scenarios for Fading Example

Scenario	$P_0$	$P_1$	$P_2$	$\tau$ (samples)	Comments
1	1.0	0	0	0	Validation
2	1.0	0.2	0	0	Ricean flat fading
3	1.0	0	0.2	0	Ricean flat fading
4	1.0	0	0.2	8	Ricean frequency selective fading
5	0	1.0	0.2	0	Rayleigh flat fading
6	0	1.0	0.2	8	Rayleigh frequency selective fading

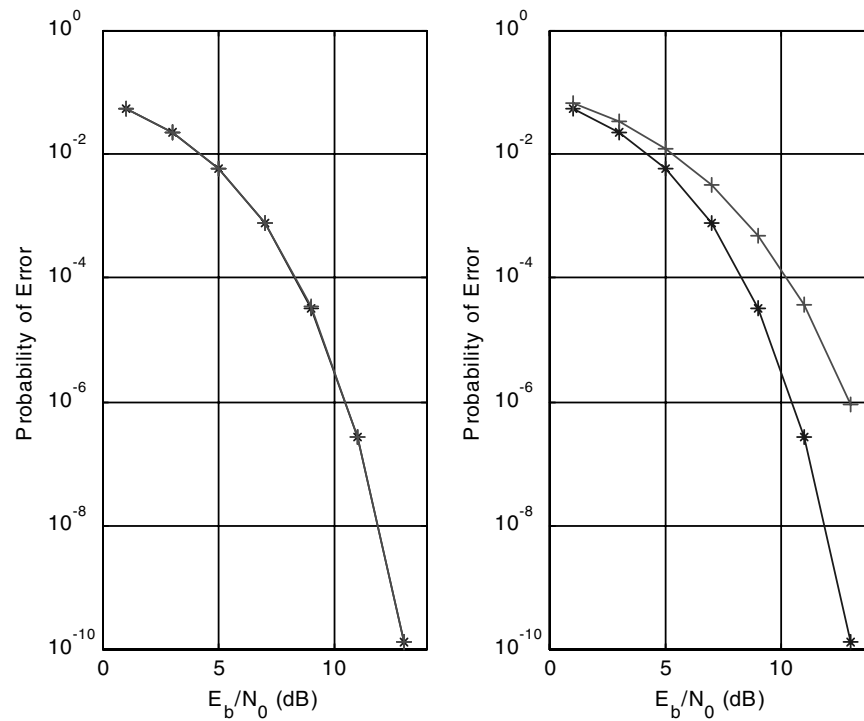
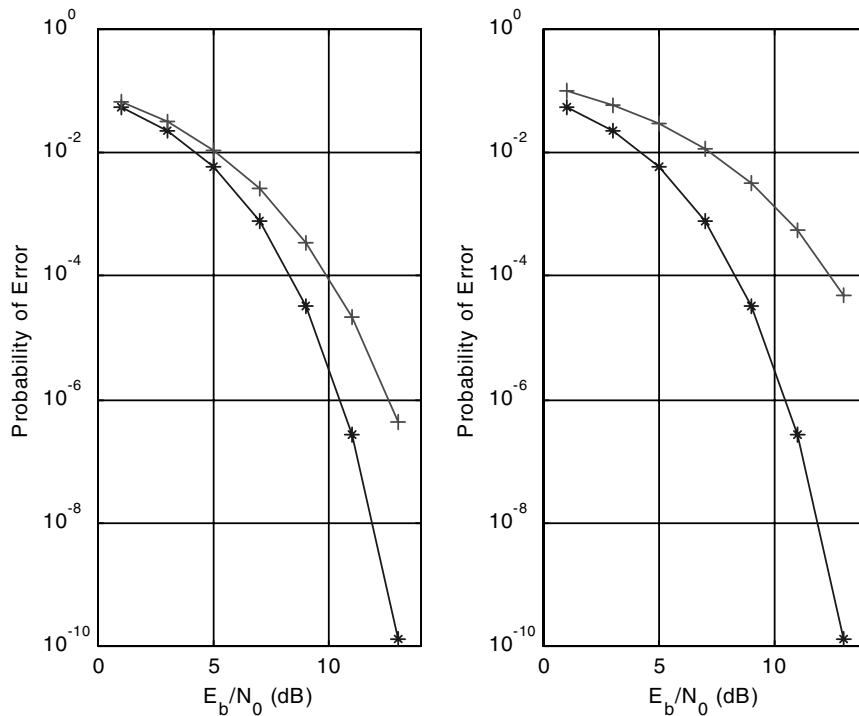


Figure 14.2 Scenario 1 (left-hand pane) and Scenario 2 (right-hand pane) illustrating the calibration run and Ricean flat fading.

frequency selective). Note the increase in BER compared to the baseline (no fading) result given in Scenario 1.

The simulation results for Scenarios 3 and 4 are illustrated in Figure 14.3. Scenario 3 is essentially equivalent to Scenario 2. The small difference is due to the fact that the fading process is different from that used in Scenario 2 due to a different initialization of the underlying random number generator. Scenario 4 is the same as Scenario 3 except that the fading is now frequency selective. Note that system performance is further degraded.

The simulation results for Scenarios 5 and 6 are illustrated in Figure 14.4. Note that for both of these scenarios there is no line-of-sight component present at the receiver input. Comparison of the Scenario 5 result with the preceding four results shows that, even for the flat-fading scenario (left-hand pane), the performance is worse than with any of the scenarios in which a line-of-sight component is present. Scenario 6 is the same as Scenario 5 except that the fading is now frequency selective. Note that system performance is further degraded. Rayleigh and Ricean channels will be explored in greater detail in the following sections. ■



**Figure 14.3** Scenario 3 (left-hand pane) and Scenario 4 (right-hand pane) illustrating Ricean flat fading and frequency selective fading.

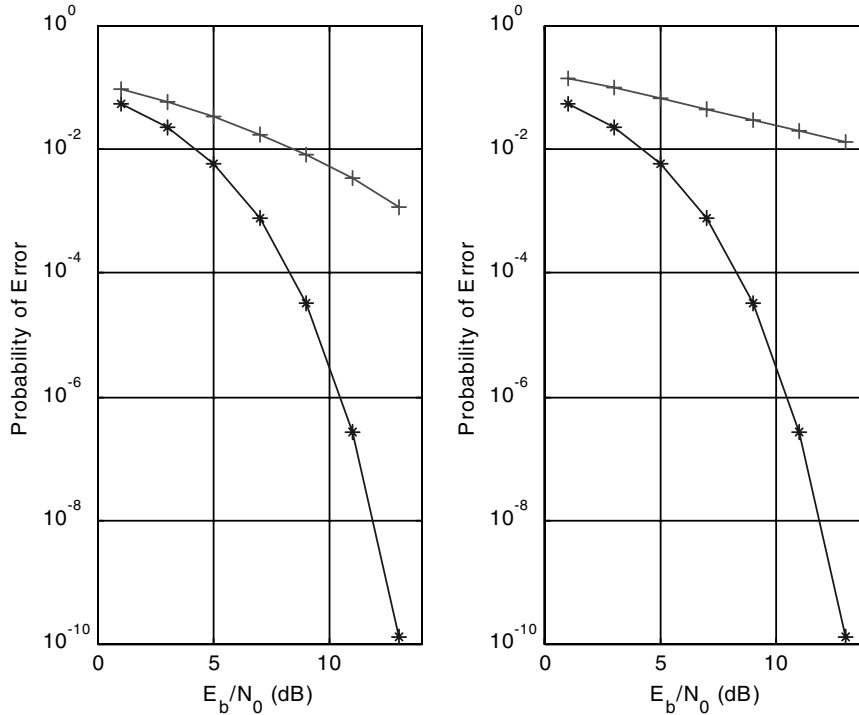


**Figure 14.4** Scenario 5 (left-hand pane) and Scenario 6 (right-hand pane) illustrating Rayleigh flat fading and frequency selective fading.

Source: M. C. Jeruchim, P. Balaban, and K. S. Shanmugan, *Simulation of Communications Systems*, 2nd ed., New York: Kluwer Academic/Plenum Publishers, 2000.

### 14.4.3 Discrete Versus Diffused Multipath

The number of multipath components will vary depending on the type of channel. In microwave communication links between fixed microwave towers using large directional antennas (narrow beams), the number of multipath components will be small, whereas in an urban mobile communication system using omnidirectional antennas, there may be a large number of multipath components caused by reflections from buildings. The same will be true for indoor wireless communications where signals can bounce off walls, furniture, and other surfaces.

There are some situations like troposcatter channels, or some mobile radio channels, where it is more appropriate to view the received signal as consisting of a continuum of multipath components rather than as a collection of discrete components. This situation is called *diffused* multipath. We will see later on in this chapter that the diffused multipath channel can be approximated by a (sampled version of) discrete multipath channel for simulation purposes.

## 14.5 Modeling Multipath Fading Channels

The recent literature on communication systems contains a vast quantity of articles dealing with the modeling and analysis of *multipath fading channels*, particularly indoor wireless and outdoor mobile channels [10–15]. While a complete review of the literature is outside the scope of this chapter, we will provide a brief review of the modeling of outdoor mobile wireless channels leading to the development of simulation techniques. These modeling and simulation techniques can be applied to other multipath fading channels.

Modeling an outdoor mobile channel is usually carried out as a two-step process which represents large-scale (macro) and small-scale (micro) effects of multipath and fading. As previously mentioned, large-scale fading represents attenuation or path loss over a large area, and this phenomenon is affected by prominent terrain features like hills, buildings, etc., between the transmitter and the receiver. The receiver is often hidden or shadowed by such terrain features, and the statistics of large-scale fading provide a way of computing the estimated signal power or path loss as a function of distance. Small-scale fading deals with large dynamic variations in the received signal amplitude and phase as a result of very small changes in the spatial separation between the transmitter and the receiver.

There are three mechanisms that affect the quality of the received signal in a mobile channel [13]: reflection, refraction, and scattering. Reflection occurs when the radio wave impinges upon a large, smooth surface (water or large metallic surfaces). Diffraction takes place when there is an obstruction in the radio path between the transmitter and receiver causing secondary radio waves to form behind the obstruction. This is called *shadowing*, and this phenomenon accounts for radio waves reaching the receive antenna even though there is no direct or line-of-sight path between the transmitter and the receiver. The third effect, scattering, results from rough surfaces whose dimensions are of the order of the wavelength, which causes the reflected energy to scatter in all directions.

While electromagnetic theory offers very complex models for these phenomena, it is possible to use simpler statistical models for the input-output relationship in a mobile channel. Specifically, the lowpass equivalent response of a mobile channel can be modeled by a complex impulse response [12] having the form

$$\tilde{h}(\tau, t) = \left\{ \left[ \frac{k}{d^n} g_{sh}(p(t)) \right]^{1/2} \right\} \tilde{c}(\tau, p(t)), \quad d > 1 \text{ km} \quad (14.28)$$

where the term in braces models the large-scale fading, and  $\tilde{c}(\tau, p(t))$  accounts for the small-scale fading as a function of the position of  $p(t)$  at time  $t$ . The constant  $K = -10 \log_{10}(k)$  is the median dB loss at a distance of 1 km. Since the reference distance is 1 km, (14.28) is only valid for  $d > 1$  km. Typically,  $K$  is of the order of 87 dB at 900 MHz,  $d$  is the distance in meters between the transmitter and the receiver, and the path loss exponent  $n$  has a value of 2 for free space (for most mobile channels its value will range from 2 to 4, with higher values applying to obstructed paths). The factor  $g_{sh}(p(t))$  accounts for shadowing due to buildings, tunnels, and other obstructions at a given location  $p(t)$ , and  $G = 10 \log_{10}(g_{sh}(p(t)))$  is usually

modeled as a Gaussian variable with a mean of 0 dB and a standard deviation of 6 to 12 dB depending upon the environment (this model is called the lognormal shadowing model (see [13] for more details). It is a common practice to express the path loss [the term in braces in (14.28)] as

$$L(d)_{dB} = L(1 \text{ km})_{dB} + 10n \log(d) + X_\sigma \quad (14.29)$$

where  $X_\sigma$  is a zero mean Gaussian variable with a standard deviation of 6 to 12 dB.

In (14.28),  $\tilde{c}(\tau, p(t))$  represents the complex lowpass equivalent impulse response of the channel at position  $p(t)$ , and the local multipath and fading that will result from small spatial displacements around the location  $p(t)$ . The path loss associated with large-scale fading, represented by the term in braces in (14.28), as well as fading due to shadowing, changes very slowly as a function of time at normal vehicular speeds compared to the rate of change of  $\tilde{c}(\tau, p(t))$ . Hence the channel attenuation due to large-scale fading and shadowing may be treated as a constant within a small local area, and the large-scale effect on system performance is reflected in the *average* received signal. The dynamic behavior of receiver subsystems such as tracking loops and equalizers, as well as the bit error rate of the system, will be affected significantly by the small-scale behavior modeled by  $\tilde{c}(\tau, p(t))$ . Hence much of the effort in the modeling and simulation of mobile wireless channels is focused on  $\tilde{c}(\tau, p(t))$ . In the following discussion we will use  $\tilde{c}(\tau, t)$  as a shorter notation for  $\tilde{c}(\tau, p(t))$ .

## 14.6 Random Process Models

A variety of models have been proposed for characterizing multipath fading channels, and almost all of them involve using random process models to characterize fading (see [15] for an example). There are two classes of models for describing multipath, the discrete multipath model (finite number of multipath components), and the diffused multipath model (continuum of multipath components). In mobile radio communications, the first model is often used for waveform-level simulation of mobile radio channels, while the second model is used for troposcatter channels having narrowband modulation. In both of these cases, the channel is modeled as a linear time-varying system with a complex lowpass equivalent response  $\tilde{c}(\tau, t)$ . If there are  $N$  discrete multipath components, the output of the channel consists of the sum of  $N$  delayed and attenuated versions of the input. Thus

$$\tilde{y}(t) = \sum_{k=1}^{N(t)} \tilde{a}_k(t) \tilde{x}(t - \tau_k(t)) \quad (14.30)$$

The impulse response  $\tilde{c}(\tau, t)$  is

$$\tilde{c}(\tau, t) = \sum_{k=1}^{N(t)} \tilde{a}_k(t) \delta(\tau - \tau_k(t)) \quad (14.31)$$

where  $N(t)$  is the number of multipath components, and  $\tilde{a}_k(t)$  and  $\tau_k(t)$  are the complex attenuation and the delay of the  $k^{\text{th}}$  multipath at time  $t$ .

As previously mentioned, a multipath channel may be time invariant. However, for all practical channels of interest, the channel may be characterized as time varying (fading). Time variations arise for two reasons:

1. The environment is changing even though the transmitter and receiver are fixed; examples are changes in the ionosphere, movement of foliage, and movement of reflectors and scatterers.
2. The transmitter and the receiver are mobile even though the environment might be static. Hence, in practical multipath channels,  $N$ ,  $a_k$ , and  $\tau_k$  may all be randomly time varying. An example is illustrated in Figure 14.5.

Random fluctuations in the received signal due to fading can be modeled by treating  $\tilde{c}(\tau, t)$  as a random process in  $t$ . If the received signal is made up of the sum of a large number of scattered components in each path, the central limit theorem leads to a model in which  $\tilde{c}(\tau, t)$  can be represented as a complex Gaussian process in  $t$ . At any time  $t$ , the probability density function of the real and imaginary parts are Gaussian. This model implies that for each  $\tau$  or  $\tau_k$ , the ray is composed of a large number of unresolvable components. Hence,  $\tilde{c}(\tau, t)$  and  $\tilde{a}_k(t)$  are both complex Gaussian processes in  $t$ .

If  $\tilde{c}(\tau, t)$  has a zero mean, the envelope  $R = |\tilde{c}(\tau, t)|$  has a Rayleigh probability density function of the form

$$f_R(r) = \frac{r}{\sigma^2} \exp\left(-\frac{r^2}{2\sigma^2}\right), \quad r > 0 \quad (14.32)$$

where  $\sigma^2$  is the variance of the real and imaginary parts of  $\tilde{c}(\tau, t)$ .

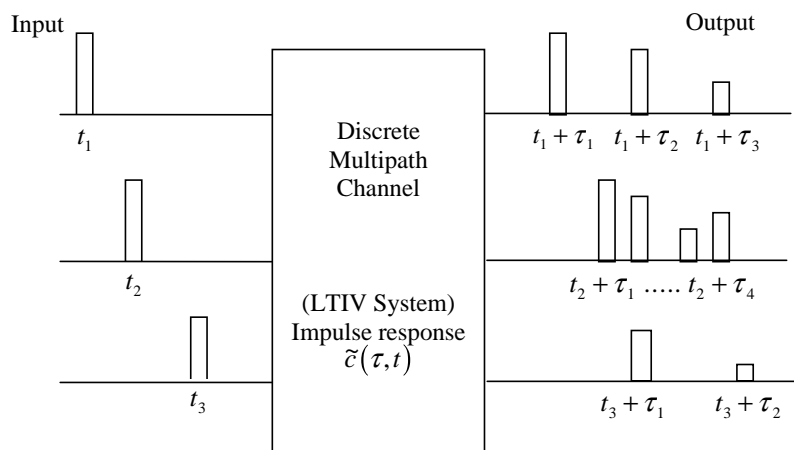


**Figure 14.5** Example of a discrete multipath fading channel.

If  $\tilde{c}(\tau, t)$  has a nonzero mean, which implies the presence of a line-of-sight non-faded path (referred to as a specular component), then  $R = |\tilde{c}(\tau, t)|$  has a Ricean probability density function of the form

$$f_R(r) = \frac{r}{\sigma^2} I_0 \left( \frac{Ar}{\sigma^2} \right) \exp \left( -\frac{r^2 + A^2}{2\sigma^2} \right), \quad r > 0 \quad (14.33)$$

where  $A$  is the nonzero mean of  $\tilde{c}(\tau, t)$ , and  $I_0(z)$  is the modified Bessel function defined by

$$I_0(z) = \frac{1}{2\pi} \int_0^{2\pi} \exp(z \cos(u)) du \quad (14.34)$$

The ratio  $K = A^2/\sigma^2$ , referred to as the Ricean factor, is an indicator of the relative power in the unfaded and faded components. Values of  $K \gg 1$  indicate less severe fading, whereas  $K \ll 1$  indicates severe fading.

The channel is called a Rayleigh fading channel or a Ricean fading channel depending on the pdf of  $|\tilde{c}(\tau, t)|$ . Other distributions for  $|\tilde{c}(\tau, t)|$  such as Nakagami and Weibul are also possible [12]. Generalized probability density functions describing envelope statistics for a finite number of specular components, together with diffuse multipath, have recently been developed [16]. In these results, Ricean and Rayleigh fading are special cases. For discrete multipath channels, these pdfs apply to  $|\tilde{a}_k(t)|$ . While the pdf of  $|\tilde{c}(\tau, t)|$  describes the instantaneous value of the complex impulse response, the temporal variations are modeled by either an appropriate autocorrelation function or power spectral density of the random process in the  $t$  variable. We describe these models now.

### 14.6.1 Models for Temporal Variations in the Channel Response (Fading)

The time-varying nature of the channel is mathematically modeled by treating  $\tilde{c}(\tau, t)$  as a *wide sense stationary* (WSS) random process in  $t$  with an autocorrelation function

$$R_{\tilde{c}\tilde{c}}(\tau_1, \tau_2, \alpha) = E \{ \tilde{c}^*(\tau_1, t) \tilde{c}(\tau_2, t + \alpha) \} \quad (14.35)$$

In most multipath channels, the attenuation and phase shift associated with different delays (i.e., paths) are assumed uncorrelated. This *uncorrelated scattering* (US) assumption leads to

$$R_{\tilde{c}\tilde{c}}(\tau_1, \tau_2, \alpha) = R_{\tilde{c}\tilde{c}}(\tau_1, \alpha) \delta(\tau_1 - \tau_2) \quad (14.36)$$

Equation (14.36) embodies both the wide sense stationary and uncorrelated scattering assumptions. It is often referred to as the WSSUS model for fading, and was originally proposed by Bello [9]. This autocorrelation function is denoted by  $R_{\tilde{c}\tilde{c}}(\tau, \alpha)$  and is given by

$$R_{\tilde{c}\tilde{c}}(\tau, \alpha) = E \{ \tilde{c}^*(\tau, t) \tilde{c}(\tau, t + \alpha) \} \quad (14.37)$$

By Fourier transforming the autocorrelation function we can obtain a frequency domain model for fading in the form of a power spectral density as

$$S(\tau, \lambda) = F \{ (R_{\tilde{c}\tilde{c}}(\tau, \alpha)) \} = \int_{-\infty}^{\infty} R_{\tilde{c}\tilde{c}}(\tau, \alpha) \exp(-j2\pi\lambda\alpha) d\alpha \quad (14.38)$$

The quantity  $S(\tau, \lambda)$  is called the scattering function of the channel, and is a function of two variables, a time domain variable (delay) and a frequency domain variable, which is called the doppler frequency variable. The scattering function provides a single measure of the average power output of the channel as a function of delay and doppler frequency.

From the scattering function we can obtain the most important parameters of the channel which impact the performance of a communication system operating over the channel. We start with the “multipath intensity” profile, defined as

$$p(\tau) = R_{\tilde{c}\tilde{c}}(\tau, 0) = E \{ |\tilde{c}(\tau, t)|^2 \} \quad (14.39)$$

which represents the average received power as a function of delay. Equation (14.39) is commonly referred to as the power-delay profile [13]. It can be shown that  $p(\tau)$  is related to the scattering function via

$$p(\tau) = \int_{-\infty}^{\infty} S(\tau, \lambda) d\lambda \quad (14.40)$$

Another function that is useful for characterizing fading is the doppler power spectrum, which is derived from the scattering function according to

$$S_d(\lambda) = \int_{-\infty}^{\infty} S(\tau, \lambda) d\tau \quad (14.41)$$

The relationships between these functions are shown in Figure 14.6.

The multipath intensity profile is usually measured by probing the channel with a wideband RF waveform where the modulating signal is a high-rate PN sequence. By crosscorrelating the receiver output against delayed versions of the PN sequence and measuring the average value of the correlator output, one can obtain the power versus delay profile. Where measurements for mobile radio applications with a fixed base station and mobile user are concerned, the power delay profile is measured in short distance increments of fractions of a wavelength. The recorded power profile is then averaged over 10 to 20 wavelengths in order to average out the effects of Rayleigh fading. The correlation measurements made as a function of position, i.e., the spatial autocorrelation function, can be converted to a temporal correlation function by noting that  $\Delta X = v\Delta t$ , where  $\Delta X$  is the incremental spatial movement of the mobile and  $v$  is the speed. Thus, the doppler spectrum can be obtained by transforming the temporal correlation function for any vehicle speed.

## 14.6.2 Important Parameters

The scattering function, the multipath intensity profile, and the doppler spectrum describe various aspects of a fading channel in detail. The two most important

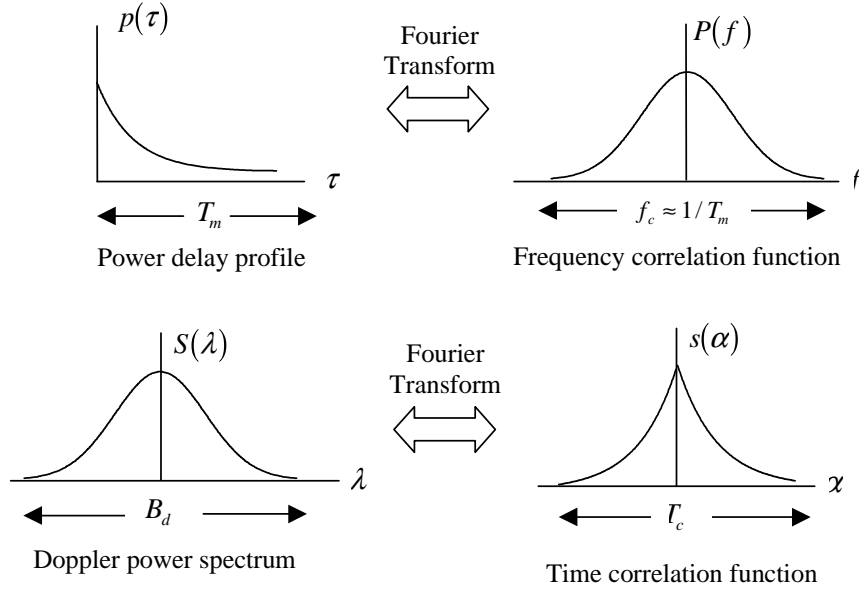


Figure 14.6 Relationship between various parts of the scattering function.

parameters, however, for simulating a fading channel are the multipath spread and the doppler bandwidth.

### Multipath Spread

Important indicators of the severity of the multipath effect are the maximum delay spread and the rms delay spread. The (maximum) delay spread which represents the value  $T_{\max}$  of the delay beyond which the received power  $p(\tau)$  is very small, and the *rms delay spread*  $\sigma_\tau$ , is defined as

$$\sigma_\tau = [\langle \tau^2 \rangle - \langle \tau \rangle^2]^{1/2} \quad (14.42)$$

where  $\langle x \rangle$  denotes the time-average value of  $x$  and

$$\langle \tau^k \rangle = \frac{\int \tau^k p(\tau) d\tau}{\int p(\tau) d\tau} \quad (14.43)$$

When the delay spread is of the order of, or greater than, the symbol duration in a digital communication system, the delayed multipath components will arrive in different symbol intervals and cause intersymbol interference, which can adversely impact the BER performance. This is equivalent to the time-varying transfer function of a channel having a bandwidth less than the signal bandwidth. In this case, the channel behaves as a bandlimiting filter and is said to be frequency selective.

For a channel that is not frequency selective, the maximum delay spread is much smaller than the symbol duration  $T_s$

$$T_{\max} \ll T_s \quad \text{or} \quad \sigma_T < 0.1T_s \quad (14.44)$$

In the nonfrequency-selective case, all of the delayed multipath components arrive within a short fraction of a symbol time. In this case, the channel can be modeled by a single ray, and the input-output relationship can be expressed as a multiplication. In other words

$$\tilde{y}(t) = \tilde{a}(t) \tilde{x}(t) \quad (14.45)$$

For a frequency-selective channel

$$T_{\max} \gg T_s \quad \text{or} \quad \sigma_T > 0.1T_s \quad (14.46)$$

and the input-output relationship is the convolution

$$\tilde{y}(t) = \tilde{c}(\tau, t) \circledast \tilde{x}(t) \quad (14.47)$$

where  $\circledast$ , as always, denotes convolution. While the delay *spread* (maximum or rms) has a significant impact on the performance of a communications system, it has been observed that the system performance is not very sensitive to the *shape* of the multipath intensity profile  $p(\tau)$ . The most commonly assumed forms for  $p(\tau)$  are uniform and exponential.

### Doppler Bandwidth

The doppler bandwidth, or the doppler spread,  $B_d$ , is the bandwidth of the doppler spectrum  $S_d(\lambda)$  as defined by (14.41), and is an indicator of how fast the channel characteristics are changing (fading) as a function of time. If  $B_d$  is of the order of the signal bandwidth  $B_s$  ( $\approx 1/T_s$ ), the channel characteristics are changing (fading) at a rate comparable to the symbol rate, and the channel is said to be fast fading. Otherwise the channel is said to be slow fading. Thus

$$\begin{aligned} B_d \ll B_s \approx 1/T_s & \quad (\text{Slow fading channel}) \\ B_d \gg B_s \approx 1/T_s & \quad (\text{Fast fading channel}) \end{aligned} \quad (14.48)$$

If the channel is slow fading, then a snapshot approach can be used to simulate the channel for performance estimation. Otherwise, the dynamic changes in the channel conditions must be explicitly simulated.

## 14.7 Simulation Methodology

We now turn our attention to the simulation of multipath fading channels. We will assume that either a discrete or diffused multipath model is specified and that the models are WSSUS. The distributions, delay profile, and the doppler spectrum, are assumed to be given. Furthermore, we will assume the fading to be Rayleigh or Ricean, with an emphasis on Rayleigh fading, since the Ricean model can be obtained from the Rayleigh model by adding a nonzero mean. We begin with the diffused multipath channel.

### 14.7.1 Simulation of Diffused Multipath Fading Channels

The diffused multipath channel is a linear time-varying system that is characterized by a continuous, rather than discrete, time-varying impulse response  $\tilde{c}(\tau, t)$ . The simulation model for an LTV system was derived in Chapter 13 and we repeat only the essential steps here. Since the lowpass input to the channel can be assumed to be bandlimited to a bandwidth  $B$  of the order  $r/2$ , where  $r$  is the symbol rate ( $B \approx r$  for the bandpass case), we can represent the lowpass input in terms of its sampled values using the minimum sampling rate of  $r$  samples per second as

$$\tilde{x}(t - \tau) = \sum_{n=-\infty}^{\infty} \tilde{x}(t - nT) \frac{\sin(2\pi B(\tau - nT))}{2\pi B(\tau - nT)} \quad (14.49)$$

where  $T = 1/r$  is the time between samples. Substituting the above representation of  $\tilde{x}(t - \tau)$  in the convolution integral

$$\tilde{y}(t) = \int_{-\infty}^{\infty} \tilde{c}(\tau, t) \tilde{x}(t - \tau) d\tau \quad (14.50)$$

we obtain

$$\begin{aligned} \tilde{y}(t) &= \int_{-\infty}^{\infty} \tilde{c}(\tau, t) \left\{ \sum_{n=-\infty}^{\infty} \tilde{x}(t - nT) \frac{\sin(2\pi B(\tau - nT))}{2\pi B(\tau - nT)} \right\} d\tau \\ &= \sum_{n=-\infty}^{\infty} \tilde{x}(t - nT) \int_{-\infty}^{\infty} \tilde{c}(\tau, t) \left\{ \frac{\sin(2\pi B(\tau - nT))}{2\pi B(\tau - nT)} \right\} d\tau \end{aligned} \quad (14.51)$$

Thus

$$\tilde{y}(t) = \sum_{n=-\infty}^{\infty} \tilde{x}(t - nT) \tilde{g}_n(t) \quad (14.52)$$

where

$$\tilde{g}_n(t) = \int_{-\infty}^{\infty} \tilde{c}(\tau, t) \left\{ \frac{\sin(2\pi B(\tau - nT))}{2\pi B(\tau - nT)} \right\} d\tau \quad (14.53)$$

Simulation models for diffused multipath fading channels are derived from (14.52) using two approximations. Truncating the sum in (14.52) so that only the terms for which  $|n| \leq m$  are included and approximating the integral in (14.53) as

$$\tilde{g}_n(t) \approx T \tilde{c}(nT, t) \quad (14.54)$$

leads to the computationally efficient form

$$\begin{aligned} \tilde{y}(t) &= \sum_{n=-\infty}^{\infty} \tilde{x}(t - nT) \tilde{g}_n(t) \approx \sum_{n=-m}^m \tilde{x}(t - nT) \tilde{g}_n(t) \\ &\approx T \sum_{n=-m}^m \tilde{x}(t - nT) \tilde{c}(nT, t) \end{aligned} \quad (14.55)$$

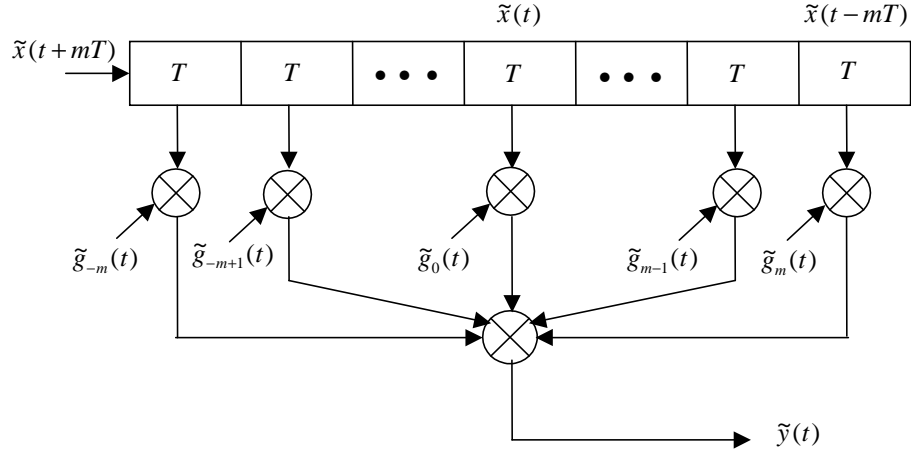


**Figure 14.7** TDL model for a diffused multipath channel with  $\tilde{g}_n(t) = T\tilde{c}(nT, T)$ .

Source: M. C. Jeruchim, P. Balaban, and K. S. Shanmugan, *Simulation of Communications Systems*, 2nd ed., New York: Kluwer Academic/Plenum Publishers, 2000.

Equation (14.55) can be implemented using a tapped delay line as shown in Figure 14.7.

For a Rayleigh fading channel, the tap gain processes  $\tilde{g}_n(t) \approx T\tilde{c}(nT, t)$  are zero mean complex Gaussian processes. They will be uncorrelated because of the WSSUS assumption. The power spectral density of each tap gain process is specified by the doppler spectrum, and the variance  $\sigma_n^2$  of the  $n^{\text{th}}$  tap gain process is given by

$$E\{|\tilde{g}_n(t)|^2\} \approx \sigma_n^2 = T^2 E\{|\tilde{c}(nT, t)|^2\} = T^2 p(nT) \quad (14.56)$$

and is obtained from the sampled values of the multipath intensity profile  $p(\tau)$ , an example of which is shown in Figure 14.8, where the total number of taps is  $T_{\text{max}}/T$ .

### Special Cases

If the channel is time invariant, then  $\tilde{c}(\tau, t) = \tilde{c}(\tau)$ , and the tap gains become constants. Therefore

$$\tilde{g}_n(t) = \tilde{g}_n \approx T\tilde{c}(nT) \quad (14.57)$$

In other words, the tap gains are sampled values of the impulse response of the LTIV system, and the tapped delay line model reduces to an FIR filter performing time-domain convolution. If the channel is frequency nonselective, then there is only one tap in the model, and  $\tilde{y}(t) = \tilde{x}(t)\tilde{g}(t)$ , where  $\tilde{g}(t)$  is either a Rayleigh or Ricean process.

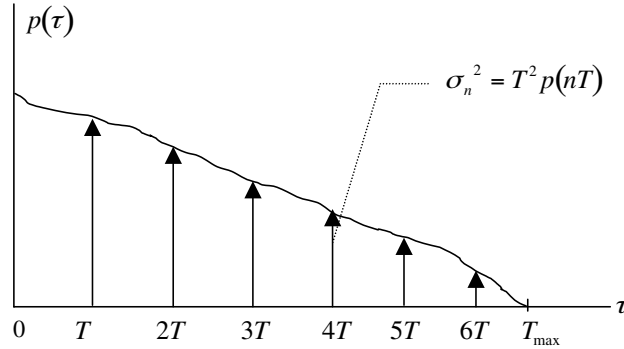


**Figure 14.8** Sampled values of the power delay profile.

Source: M. C. Jeruchim, P. Balaban, and K. S. Shanmugan, *Simulation of Communications Systems*, 2nd ed., New York: Kluwer Academic/Plenum Publishers, 2000.

### Sampling

An important aspect of the TDL model that deserves additional attention is the sampling rate for simulations. The TDL model shown in Figure 6.8 was derived with continuous time input  $\tilde{x}(t)$  and output  $\tilde{y}(t)$ . However, in simulation we use sampled values of  $\tilde{x}(t)$  and output  $\tilde{y}(t)$  which should be sampled at 8 to 32 times the bandwidth, where the bandwidth includes the effect of spreading due to the time-varying nature of the system as defined in Chapter 13. Note that the Nyquist rate of  $2B$ ,  $B = r/2$  was used to derive the TDL model, and the tap spacing of  $T = 1/r$  will be much greater than  $T_s$ , where  $T_s$  is the sampling time for the input and output waveforms. It is of course possible to derive a TDL model with a smaller tap spacing (i.e., more samples per symbols), but such a model will be computationally inefficient and does not necessarily improve the accuracy of the simulation.

### Generation of Tap Gain Processes

The tap gain processes are stationary random processes with Gaussian probability density functions and arbitrary power spectral density functions. The simplest model for the tap gain processes assume them to be uncorrelated, complex, zero mean Gaussian processes with different variances but identical power spectral densities. In this case, the tap gain processes can be generated by filtering white Gaussian processes, as shown in Figure 14.9.

The filter transfer function is chosen such that it produces the desired doppler power spectral density. In other words,  $H(f)$  is chosen such that

$$S_{\tilde{g}\tilde{g}}(f) = S_d(f) = S_{\tilde{w}\tilde{w}}(f) |\tilde{H}(f)|^2 = |\tilde{H}(f)|^2 \quad (14.58)$$

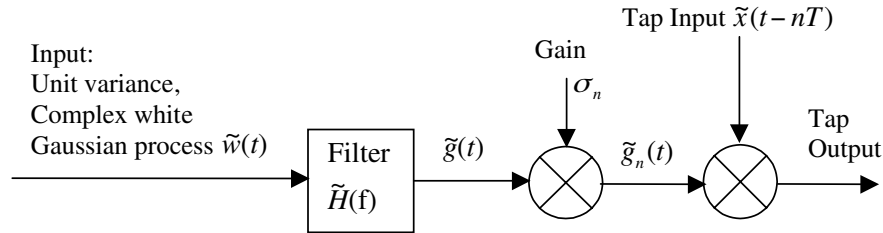


**Figure 14.9** Generation of the  $n^{\text{th}}$  tap gain process.

*Source:* M. C. Jeruchim, P. Balaban, and K. S. Shanmugan, *Simulation of Communications Systems*, 2nd ed., New York: Kluwer Academic/Plenum Publishers, 2000.

where  $S_{\tilde{w}\tilde{w}}(f)$  is the power spectral density of the input white noise process, which can be set equal to 1, and  $S_{\tilde{g}\tilde{g}}(f)$  is the specified doppler power spectral density of the tap gain processes. The filter gain is chosen such that  $\tilde{g}(t)$  has a normalized power of 1. The static gain  $\sigma_n$  in Figure 14.9 accounts for the different power levels or variances for the different taps. If the power spectral density of the tap gains are different, then different filters will be used for different taps.

### Delay Power Profiles and Doppler Power Spectral Densities

As previously mentioned, the BER performance of a communication system is more sensitive to the values of the rms and maximum delay spreads than to the shape of the power delay profile. Therefore, simple profiles such as uniform or exponential can be used for simulation. The delay profiles are normalized to have unit area (i.e., total normalized power, or the area under the locally averaged power delay profile, is set equal to one). Thus

$$\int_0^{T_m} p(\tau) dt = 1 \quad (14.59)$$

Typical rms delay spreads are given in Table 14.2.

The most commonly used models for doppler power spectral densities for mobile applications assume that there are many multipath components, each having different delays, and that all components have the same doppler spectrum. Each

**Table 14.2** Typical rms Delay Spreads

Link Type	Link Distance	rms Delay Spread
Troposcatter	100 Km	milliseconds ( $10^{-3}$ )
Outdoor Mobile	1 Km	microseconds ( $10^{-6}$ )
Indoor	10 m	nanoseconds ( $10^{-9}$ )

multipath component (ray) is actually made up of a large number of simultaneously arriving unresolvable multipath components, having angle of arrival with a uniform angular distribution at the receive antenna. This channel model was used by Jakes and others at Bell Laboratories to derive the first comprehensive mobile radio channel model for both doppler effects and amplitude fading effects [11]. The classical Jakes' doppler spectrum has the form, which was initially simulated in Chapter 7 (see Example 7.11),

$$S_d(f) = S_{\tilde{g}_n \tilde{g}_n}(f) = \frac{K}{\sqrt{1 - (f/f_d)^2}}, \quad -f_d \leq f \leq f_d \quad (14.60)$$

where  $f_d = v/\lambda$  is the maximum doppler shift,  $v$  is the vehicle speed in meters per second, and  $\lambda$  is the wavelength of the carrier. While the doppler spectrum defined by (14.60) is appropriate for dense scattering environments like urban areas, a "Ricean spectrum" is recommended for rural environments in which there is one strong direct line-of-sight path and hence Ricean fading. The Ricean doppler spectrum has the form

$$S_d(f) = S_{\tilde{g}_n \tilde{g}_n}(f) = \frac{0.41}{\sqrt{1 - (f/f_d)^2}} + 0.91\delta(f \pm 0.7f_d), \quad -f_d \leq f \leq f_d \quad (14.61)$$

and is shown in Figure 14.10. Other spectral shapes used for the doppler power spectral densities include Gaussian and uniform. Typical doppler bandwidths in mobile applications at 1 GHz will range from 10 to 200 Hz.

There are several ways of implementing the doppler spectral shaping filter needed to generate the tap gain processes in the TDL model for the channel when using the model assumed by Jakes. An FIR filter in time domain is the most common implementation, since doppler power spectral densities do not lend themselves easily to implementation in recursive form. The generation of a Jakes spectrum using FIR filtering techniques was illustrated in Chapter 7. A block processing model based on frequency domain techniques is discussed in [13].

In generating the tap gain processes it should be noted that the bandwidth of the tap gain processes for slowly time-varying channels will be very small compared

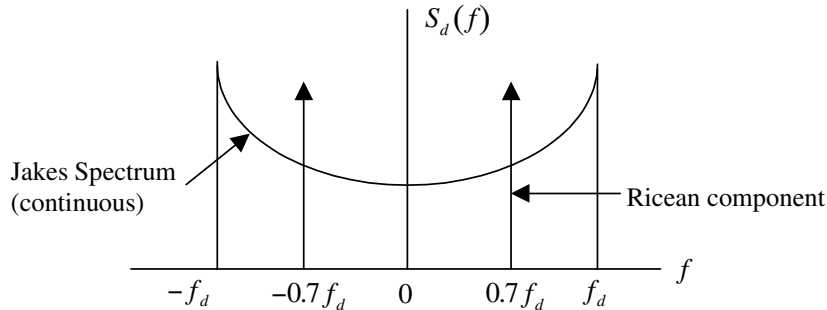


**Figure 14.10** Example of doppler power spectral densities.

to the bandwidth of the signals that flow through them. In this case, the tap gain filter should be designed and executed at a slower sampling rate. Interpolation can be used at the output of the filter to produce denser samples at a rate consistent with the sampling rate of the signal coming into the tap. Designing the filter at the higher rate will lead to computational inefficiencies as well as stability problems.

### Correlated Tap Gain Model

The approximation of the tap gain processes given in (14.53) and (14.54) by

$$\tilde{g}_n(t) = \int_{-\infty}^{\infty} \tilde{c}(\tau, t) \left\{ \frac{\sin(2\pi B(\tau - nT))}{2\pi B(\tau - nT)} \right\} d\tau \approx T\tilde{c}(nT, t) \quad (14.62)$$

leads to uncorrelated tap gain functions. Without the approximation, the tap gain functions will be correlated. It can be shown that the correlation between  $g_n(t)$  and  $g_m(t)$  is given by

$$\begin{aligned} R_{m,n}(\eta) &= E \{g_m^*(t)g_n(t + \eta)\} \\ &= \int R_{\tilde{c}\tilde{c}}(\tau, \eta) \operatorname{sinc}(2B\tau - m) \operatorname{sinc}(2B\tau - n) d\tau \end{aligned} \quad (14.63)$$

where  $T = 1/2B$  is the tap spacing.

Generating a set of correlated random processes with arbitrary power spectral density functions is very difficult. An approximation that simplifies this problem somewhat makes the reasonable assumption that all tap gain functions have the same power spectral density. Therefore, we assume that

$$S(\tau, \lambda) = m(\tau) S_d(\lambda) \quad (14.64)$$

where  $S(\tau, \lambda)$  is the scattering function,  $m(\tau)$  is the normalized power delay power profile, and  $S_d(\lambda)$  is the doppler spectrum. The solution to this case may be found in [17].

An approach to solving the general problem has been recently proposed [18]. This method is based on fitting a vector ARMA model to the tap gain processes and deriving the vector ARMA model from the given correlations and power spectral densities. The procedure for fitting the vector ARMA model is very complex, and it is not clear whether the extra work required can be justified in terms of the improvement in accuracy.

### 14.7.2 Simulation of Discrete Multipath Fading Channels

Compared to the diffused multipath model, simulation of the discrete multipath model is rather straightforward, at least conceptually. We must keep in mind that since the channel is dynamic in both space and time, care must be used to avoid aliasing [19]. The input-output relationship of a discrete multipath model is given by

$$\tilde{y}(t) = \sum_{k=1}^{N(t)} \tilde{a}_k(t) \tilde{x}(t - \tau_k(t)) \quad (14.65)$$

where  $\tilde{a}_k(t)$  is the complex path attenuation as discussed in Section 14.4. In (14.65) it can be assumed that the number of multipath components and the delay structure will vary slowly compared to the variations in  $\tilde{a}_k(t)$ . Hence the delays  $\tau_k(t)$  can be treated as constants over the duration of a simulation, and the preceding equation can be written as

$$\tilde{y}(t) = \sum_{k=1}^{N(t)} \tilde{a}_k(t) \tilde{x}(t - \tau_k) \quad (14.66)$$

and implemented in block diagram form as shown in Figure 14.11.

In order to illustrate the basic approach for simulating discrete channel models we assume that the model is specified in terms of probability distributions for the number of components  $N$ , the delays, and the complex attenuations as a function of the delays. A representation (snapshot) of the channel is then obtained as follows:

1. Draw a random number  $N$  to obtain the number of delays.
2. Draw a set of  $N$  random numbers from the distribution for delay values.
3. Draw a set of  $N$  attenuations based on the delay values.

This set of  $3N$  random numbers represents a snapshot of the channel, which is implemented as shown in Figure 14.11. In Figure 14.11 the initial delay is  $\Delta_1 = \tau_1$ . The remaining delays  $\Delta_n$ ,  $2 \leq n \leq N$ , are differential delays defined by

$$\Delta_n = \tau_n - \tau_{n-1}, \quad 2 \leq n \leq N \quad (14.67)$$

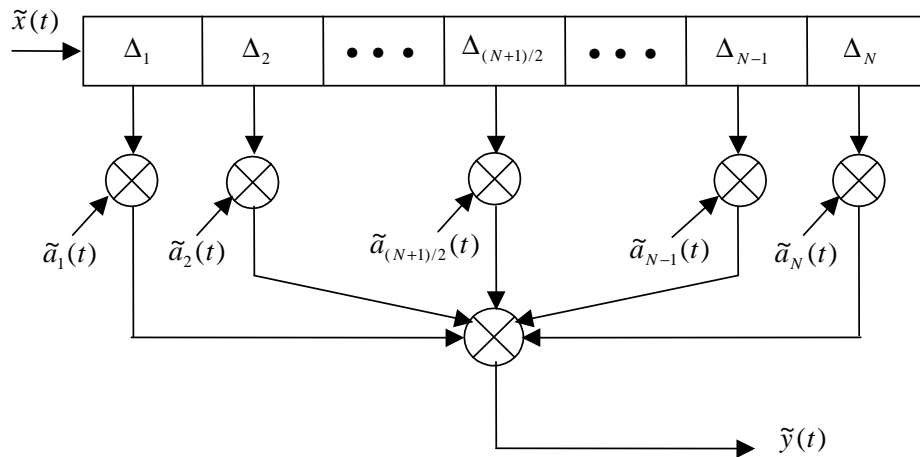


**Figure 14.11** A variable delay TDL model for discrete multipath channels.

Source: M. C. Jeruchim, P. Balaban, and K. S. Shanmugan, *Simulation of Communications Systems*, 2nd ed., New York: Kluwer Academic/Plenum Publishers, 2000.

While the implementation shown in Figure 14.11 is rather straightforward, it poses a problem when the delays differ by very small time offsets. Since everything will be sampled, the tap spacings (i.e., the differential delays  $\tau_n - \tau_{n-1}$ ) must be expressed in terms of an integer number of sampling periods for simulation. Hence, the sample time must be very small, smaller than the smallest differential delay. This might lead to excessive sampling rates and an unacceptable computational burden. We can avoid this problem by developing a TDL model with uniform tap spacing following the approach used in the simulation of diffused multipath channels in Section 14.7.1.

### Uniformly Spaced TDL Model for Discrete Multipath Fading Channels

The tap gains of a uniformly spaced TDL model are given in (14.53) as

$$\tilde{g}_n(t) = \int_{-\infty}^{\infty} \tilde{c}(\tau, t) \left\{ \frac{\sin(2\pi B(\tau - nT))}{2\pi B(\tau - nT)} \right\} d\tau \quad (14.68)$$

Substituting the impulse response of the discrete multipath channel, given by

$$\tilde{c}(\tau, t) = \sum_{k=1}^N \tilde{a}_k(t) \delta(\tau - \tau_k) \quad (14.69)$$

in the preceding equation, we obtain the tap gains as

$$\tilde{g}_n(t) = \sum_{k=1}^N \tilde{a}_k(t) \operatorname{sinc}\left(\frac{\tau_k}{T} - n\right) = \sum_{k=1}^N \tilde{a}_k(t) \alpha(k, n) \quad (14.70)$$

In (14.70)

$$\alpha(k, n) = \operatorname{sinc}\left(\frac{\tau_k}{T} - n\right) \quad (14.71)$$

Note that the envelope of  $\alpha(k, n)$  decreases as  $|n|$  increases. Hence the number of taps can be truncated to  $|n| \leq m$ , where  $m$  is chosen to satisfy  $m \gg T_{\max}T$ . For the case where the maximum delay spread  $T_{\max}$  will not exceed 3 or 4 symbol times, the number of taps need not be greater than about 20 ( $-m < n < m$ ,  $m = 10$ ). The model now takes the form previously derived for the approximate diffused multipath model illustrated in Figure 14.7.

The generation of the tap gains is illustrated in Figure 14.12. Note that the generation of the tap gain processes for the discrete multipath model is straightforward compared to the generation of the tap gain processes for the diffused case. We start with a set of  $N$  independent, zero-mean complex Gaussian white noise processes, which are filtered to produce the appropriate doppler spectrum. These are then scaled to produce the desired power profile, and are finally transformed according to (14.70) to produce the tap gain processes. (Note that only two of the  $N$  paths are shown in Figure 14.12.)

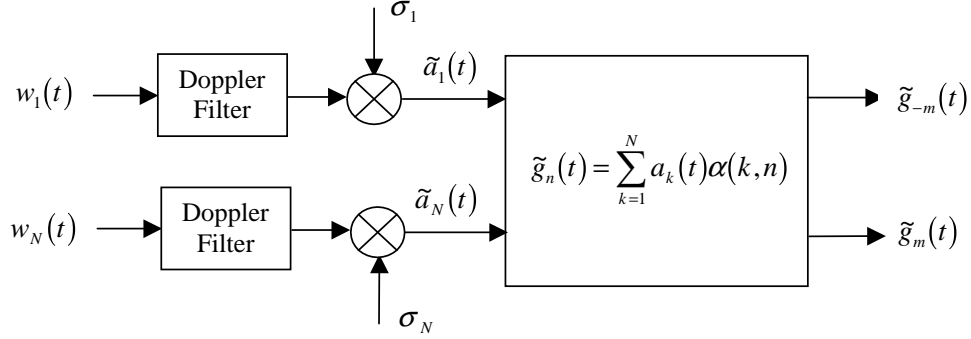


**Figure 14.12** Generation of the tap gain processes.

Source: M. C. Jeruchim, P. Balaban, and K. S. Shanmugan, *Simulation of Communications Systems*, 2nd ed., New York: Kluwer Academic/Plenum Publishers, 2000.

To illustrate the calculation of the tap gain functions let us assume that

$$\Delta\tau = \frac{\tau_2 - \tau_1}{T} = 0.5 \quad (14.72)$$

The tap gain functions in this case are obtained by filtering two uncorrelated white Gaussian noise processes and then transforming them to tap gain processes according to (14.70) as

$$\begin{bmatrix} \tilde{g}_{-4}(t) \\ \tilde{g}_{-3}(t) \\ \tilde{g}_{-2}(t) \\ \tilde{g}_{-1}(t) \\ \tilde{g}_0(t) \\ \tilde{g}_1(t) \\ \tilde{g}_2(t) \\ \tilde{g}_3(t) \\ \tilde{g}_4(t) \end{bmatrix} = \begin{bmatrix} \text{sinc}(0.0 + 4) & \text{sinc}(0.5 + 3) \\ \text{sinc}(0.0 + 3) & \text{sinc}(0.5 + 3) \\ \text{sinc}(0.0 + 2) & \text{sinc}(0.5 + 2) \\ \text{sinc}(0.0 + 1) & \text{sinc}(0.5 + 1) \\ \text{sinc}(0.0) & \text{sinc}(0.5) \\ \text{sinc}(0.0 - 1) & \text{sinc}(0.5 - 1) \\ \text{sinc}(0.0 - 2) & \text{sinc}(0.5 - 2) \\ \text{sinc}(0.0 - 3) & \text{sinc}(0.5 - 3) \\ \text{sinc}(0.0 - 4) & \text{sinc}(0.5 - 4) \end{bmatrix} \begin{bmatrix} \tilde{a}_1(t) \\ \tilde{a}_2(t) \end{bmatrix} \quad (14.73)$$

which is

$$\begin{bmatrix} \tilde{g}_{-4}(t) \\ \tilde{g}_{-3}(t) \\ \tilde{g}_{-2}(t) \\ \tilde{g}_{-1}(t) \\ \tilde{g}_0(t) \\ \tilde{g}_1(t) \\ \tilde{g}_2(t) \\ \tilde{g}_3(t) \\ \tilde{g}_4(t) \end{bmatrix} = \begin{bmatrix} 0.0 & 0.0707 \\ 0.0 & -0.0910 \\ 0.0 & 0.1273 \\ 0.0 & -0.2122 \\ 1.0 & 0.6366 \\ 0.0 & 0.6366 \\ 0.0 & -0.2122 \\ 0.0 & 0.1273 \\ 0.0 & -0.0909 \end{bmatrix} \begin{bmatrix} \tilde{a}_1(t) \\ \tilde{a}_2(t) \end{bmatrix} \quad (14.74)$$

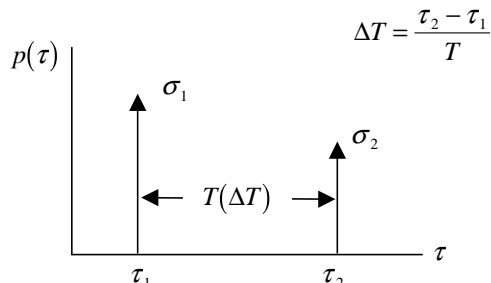


**Figure 14.13** Simple two-ray model. (Note that  $\Delta\tau$  is normalized).

*Source:* M. C. Jeruchim, P. Balaban, and K. S. Shanmugan, *Simulation of Communications Systems*, 2nd ed., New York: Kluwer Academic/Plenum Publishers, 2000.

where  $\tilde{a}_1$  and  $\tilde{a}_2$  are defined in Figure 14.12. The preceding equation shows the coefficients of the transformation for only 9 taps. We see that these coefficients will be negligible for higher-order tap gains and, as a result, they can be ignored. The TDL model is therefore truncated to 9 taps.

A simple two-ray model is often used to make preliminary performance predictions for fading channels. Consider the power-delay profile illustrated in Figure 14.13. Parametric performance predictions can be made by varying the ratio of the normalized delay spread  $\Delta\tau = (\tau_2 - \tau_1)/T$ , where  $T$  is the symbol duration and the ratio of relative powers in the two paths  $(\sigma_1/\sigma_2)^2$ . If  $\Delta\tau \ll 0.1$ , then the two paths can be combined and the model can be treated as frequency nonselective. If  $\Delta\tau > 0.1$ , there will be considerable intersymbol interference in the channel and it is treated as frequency selective.

**Example 14.2.** In this example we consider the effect of fading due to doppler on the transmission of a QPSK signal on a discrete multipath channel. The block diagram is illustrated in Figure 14.14. The generation of the tap weights is shown in Figure 14.14(a). The doppler filter is realized using the Jakes model defined by (14.60) with  $K = 1$  and  $f_d = 100$  Hz. The tap gain processes are uncorrelated and Gaussian. The tap spacing is based on an RF bandwidth of 20 kHz (lowpass equivalent bandwidth of 10 kHz). The tap weights are denoted  $\mathbf{tw1}$  and  $\mathbf{tw2}$ . The complex signal is multiplied by the complex tap weights. Both the complex QPSK signal and the complex carrier are used as inputs. The carrier is defined by

$$c(t) = \exp[j2\pi(1000)t] \quad (14.75)$$

The delay of 8 samples corresponds to one-half of the symbol time. Additional details are included in the MATLAB code for this example, which is given in Appendix B.

The simulation length is determined from a number of considerations. In order to observe the spectra of the input and output for the complex exponential case,

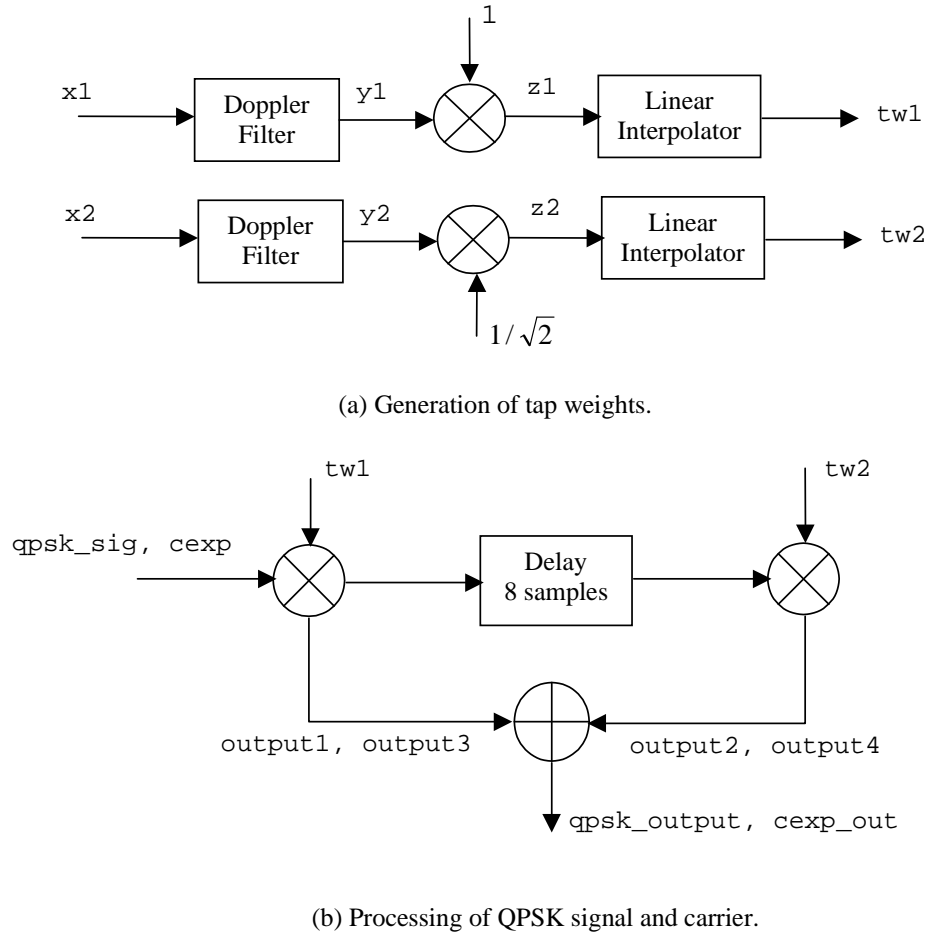


**Figure 14.14** Block diagrams of simulated systems.

10 to 20 cycles of the complex exponential are needed. At the same time, in order to capture the effects of the time-varying channel, we need to simulate the fading process for about 5 to 10 times the reciprocal of the doppler bandwidth. These two considerations lead to a simulation length of  $1/20$  second, or about 8,000 samples.

Executing the MATLAB program given in Appendix B generates the results illustrated in Figures 14.15, 14.16, and 14.17. The input and output carrier signals are shown in Figure 14.15. The input (top pane) is the tone at 1,000 Hz. The output (bottom pane) illustrates the spectral spreading due to doppler. The direct channel input and output are illustrated in Figure 14.16. The input signal (top pane) has two levels as expected. The output signal (bottom pane) has more than

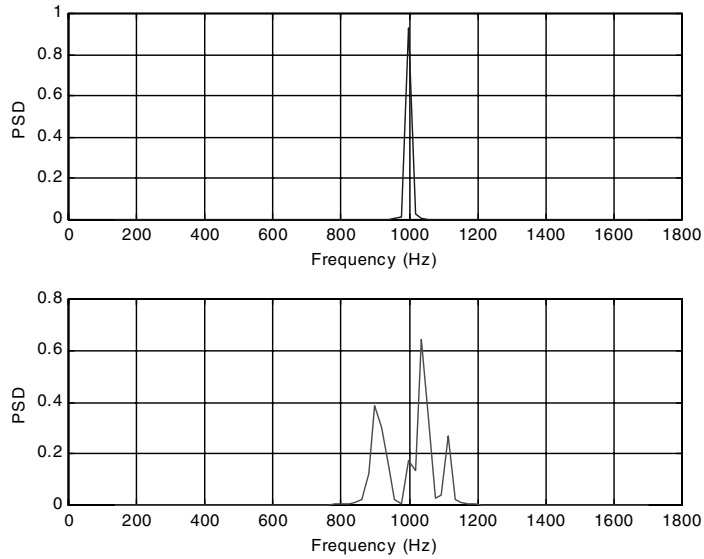


**Figure 14.15** Input (top pane) and output (bottom pane) power spectral densities. The spectral spreading due to doppler is evident in the bottom pane.

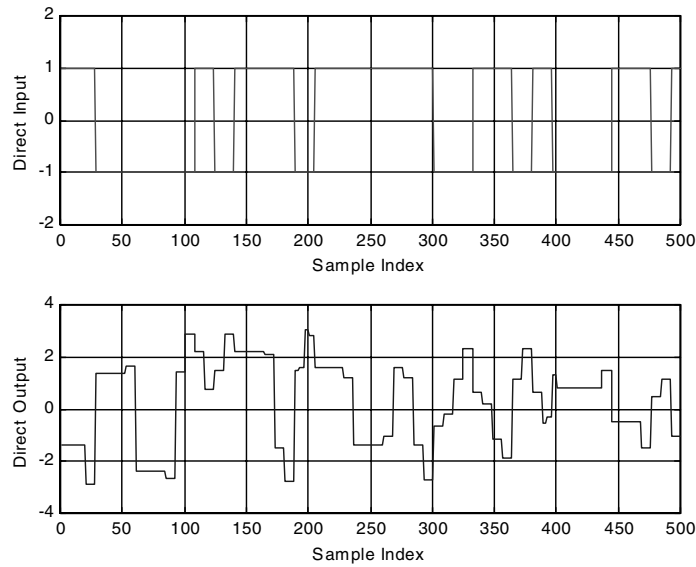


**Figure 14.16** Direct channel QPSK input and output.

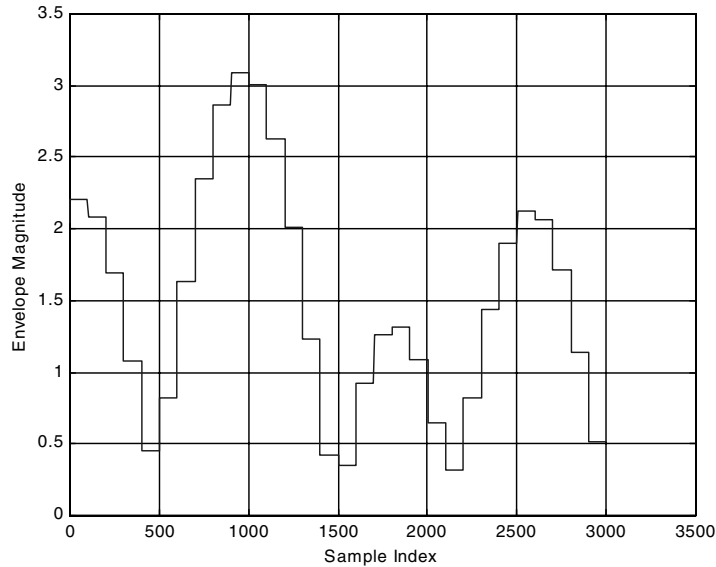


Figure 14.17 Envelope of the complex exponential output.

two levels because of intersymbol interference. The envelope of the QPSK output signal is illustrated in Figure 14.17. ■

### 14.7.3 Examples of Discrete Multipath Fading Channel Models

In this section we present a number of examples of discrete multipath models that are used to simulate the performance of wireless communication systems. The first model that we present is the so-called Rummler's model for terrestrial microwave communication links between fixed antenna towers. This is a line-of-sight radio channel with a very small number of multipath components because of the larger directional antennas used in the system and the very benign properties of the tropospheric channel used by LOS microwave radio. Larger antennas mean that the field of view of the antenna is limited at very small angles of arrival which yields a smaller number of multipath components. Also, since the antennas are fixed, the only time variations in the channel characteristics are due to changes in the atmospheric conditions. These variations can be considered very slow compared to the channel bandwidths which will be of the order of tens of MHz. Hence Rummler's model is a multipath model with very slow fading.

The second set of examples that we present are for mobile radio channels. These channels typically have a larger number of multipath components because of the use of omnidirectional antennas which pick up a large number of reflections with widely varying propagation delays, especially in urban areas. They will also experience faster fading due to the the large number of multipath components that experience

large carrier phase shifts over small distance changes and thus can combine destructively or constructively over small distances.

### Rummler's Model for LOS Terrestrial Microwave Channels

One of the most widely used models for terrestrial microwave links operating in the frequency range of 4 – 6 GHz between fixed towers, was developed by Rummler [20]. This model is based on a set of assumptions, and measured data is used to obtain numerical values of the model parameters. Given the geometry of the link and antenna parameters, Rummler hypothesized a three-ray model of the form

$$y(t) = x(t) + \alpha x(t - \tau_1) + \beta x(t - \tau_2) \quad (14.76)$$

where  $x(t)$  and  $y(t)$  are the bandpass input and output, respectively. In terms of the complex envelopes, the model takes the form

$$\tilde{y}(t) = \tilde{x}(t) + \alpha \exp(-j2\pi f_c \tau_1) \tilde{x}(t - \tau_1) + \beta \exp(-j2\pi f_c \tau_2) \tilde{x}(t - \tau_2) \quad (14.77)$$

and the lowpass equivalent transfer function of Rummler's channel is given by

$$H(f) = 1 + \alpha \exp(-j2\pi(f_c - f)\tau_1) + \beta \exp(-j2\pi(f_c - f)\tau_2) \quad (14.78)$$

The first simplification of the model is based on the assumption that over the bandwidth of interest  $(f_c - f)\tau_1 \ll 1$ , and hence  $\exp(-j2\pi(f_c - f)\tau_1) \approx 1$  and

$$H(f) \approx 1 + \alpha + \beta \exp(-j2\pi(f_c - f)\tau_2) \quad (14.79)$$

The next step is to assume that the “notch” frequency, where the magnitude of the response is minimum, is  $f_c + f_0$  in the bandpass case, and at  $f_0$  in the lowpass model, so that the final form of the lowpass equivalent transfer function can be written as

$$H(f) \approx a[1 - b \exp(-j2\pi(f_0 - f)\tau_2)] \quad (14.80)$$

where  $a = 1 + \alpha$  is the overall attenuation, and  $b = -\beta / (1 + \alpha)$  is a shape parameter. The value of the delay parameter  $\tau_2$ , chosen to fit the measured data, has a value of  $\tau_2 = \tau = 6.3$  ns. Note that this small time delay is only on the order of 2 meters of propagation delay, which is physically plausible and corresponds to typical refractive path differences observed over tropospheric channels for LOS microwave radio at 2–6 GHz.

The amplitude response of the Rummler model is

$$|H(f)|^2 = a^2[1 + b^2 - 2b \cos(2\pi(f - f_0)\tau)] \quad (14.81)$$

and an example of the magnitude response is shown in Figure 14.18.

The parameters  $a$  and  $b$  are normalized and expressed in dB units as illustrated in Table 14.3. Analysis of channel data yields exponential distributions for  $B_1$

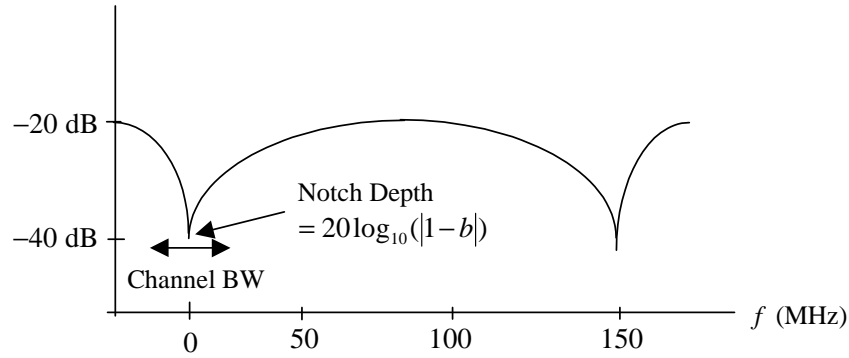


Figure 14.18 Example of the magnitude response of the Rummier channel.

Table 14.3 Parameters for Rummier Model

Minimum Phase Case ( $b < 1$ )	Nonminimum Phase Case ( $b > 1$ )
$A_1 = 20 \log_{10}(a)$	$A_2 = -20 \log_{10}(ab)$
$B_1 = 20 \log_{10}(1 - b)$	$B_2 = 10 \log_{10}(1 - 1/b)$

and  $B_2$  with means of 3.8 dB. Likewise,  $A_1$  and  $A_2$  are Gaussian with standard deviations of 5 dB. The means are

$$\mu = 24.6 \left( \frac{B^4 + 500}{B^4 + 800} \right)$$

where  $B = B_1$  for  $A_1$  and  $B = B_2$  for  $A_2$ . The probability density function of  $\theta = 2\pi f_0 \tau$  is shown in Figure 14.19.

In order to simulate a snapshot of the Rummier channel, we draw the following

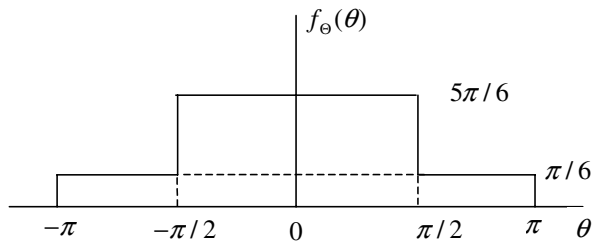


Figure 14.19 Probability density function of  $\theta$ .

set of random numbers:

1. Draw a number  $U$  uniformly distributed in  $[0,1]$ . If  $U > 0.5$ , assume minimum phase. If  $U < 0.5$ , assume nonminimum phase. (Minimum phase and nonminimum phase fades are assumed equally likely.)
2. Draw an exponentially distributed random number for  $B_1$  or  $B_2$ .
3. Draw a Gaussian random number for  $A_1$  or  $A_2$  using the value of  $B_1$  or  $B_2$ .
4. Draw a random number for  $\theta$  and set the notch frequency at  $f_0 = \theta/2\pi\tau$ ,  $\tau = 6.3ns$ .

These parameters define a snapshot of the Rummmler channel. Since the channel is assumed to be slowly varying with respect to the symbol rate, a series of snapshots of the channel is adequate for performance evaluation using a Monte Carlo simulation for each snapshot produced by the model.

### Models for Mobile Channels

Discrete channel models are also widely used for indoor and outdoor wireless channels. Many models are based on empirical data collected over a wide range of environments [21, 22, 23]. Given the large number of both mathematical and empirical models that have been proposed recently, the designer of a communication system is faced with the difficult problem of choosing a representative set of channel models that will represent the channels over which the communication system is to operate satisfactorily. Fortunately, some guidance on the choice of which models to use has been provided by international standards bodies that specify a set of “representative” channels for analyzing and simulating the performance of different types of communication systems. We present two examples below.

**Discrete Channel Models for GSM Applications** The Global System for Mobile Communications (GSM) is a standard for mobile communications in the frequency band from 1 to 2 GHz and uses 200 kHz RF channels for time-division multiplexed communications [13, 24]. The symbol time in GSM is of the order of a few microseconds.

The recommended GSM models are discrete models consisting of 12 rays (paths), and are specified for three different scenarios: rural, hilly, and urban. For each scenario, two models are specified. In addition to the 12-ray models, a simpler set of models with 6 rays (paths) are also defined. The 12-ray and 6-ray models for urban areas are given in Table 14.4 and Table 14.5, respectively. In addition to these models, there is also a model specified for testing the performance of the Viterbi equalizer used in GSM systems. This model is given in Table 14.6. All of the relative powers are in dB, and (1) and (2) designate the two equivalent models.

It should be noted that the symbol time in the system is of the order of a few microseconds, and some of the differential delays are of the order of  $0.1\mu s$ , which means that a sampling rate of 10 M samples/sec should be used in order to represent these small delays. Another approach, as outlined in the preceding

**Table 14.4** Typical Profile for Urban Areas (12-ray model)

Ray	Relative Time (1) s	Relative Time (2) s	Average Power (1) dB	Average Power (2) dB	Dopp. Spect.
1	0.0	0.0	-4.0	-4.0	Jakes
2	0.1	0.2	-3.0	-3.0	Jakes
3	0.3	0.4	0.0	0.0	Jakes
4	0.5	0.6	-2.6	-2.0	Jakes
5	0.8	0.8	-3.0	-3.0	Jakes
6	1.1	1.2	-5.0	-5.0	Jakes
7	1.3	1.4	-7.0	-7.0	Jakes
8	1.7	1.8	-5.0	-5.0	Jakes
9	2.3	2.4	-6.5	-6.0	Jakes
10	3.1	3.0	-8.6	-9.0	Jakes
11	3.2	3.2	-11.0	-11.0	Jakes
12	5.0	5.0	-10.0	-10.0	Jakes

**Table 14.5** Reduced Profile for Urban Areas (6-ray model)

Ray	Relative Time (1) s	Relative Time (2) s	Average Power (1) dB	Average Power (2) dB	Dopp. Spect.
1	0.0s	0.0s	-3.0	-3.0	Jakes
2	0.2	0.2	0.5	0.0	Jakes
3	0.5	0.6	-2.0	-2.0	Jakes
4	1.6	1.6	-6.0	-6.0	Jakes
5	2.3	2.4	-8.0	-8.0	Jakes
6	5.0	5.0	-10.0	-10.0	Jakes

**Table 14.6** Profile for Equalization Test

Ray	Relative Time	Average Power	Doppler Spectrum
1	0.0s	0.0dB	Jakes
2	3.2	0.0	Jakes
3	6.4	0.0	Jakes
4	9.6	0.0	Jakes
5	12.8	0.0	Jakes
6	16.0	0.0	Jakes

**Table 14.7** Parameters for a 3-Ray Outdoor Model for PCS

Environment	$\tau_1$ (ns)	$\tau_2$ (ns)	$\tau_3$ (ns)	Doppler	Doppler BW
Pedestrian	0	1,500	14,500	Flat	12Hz
Wireless Loop	0	1,500	14,500	Gaussian	12Hz
Vehicular	0	1500	15,500	Jakes	180Hz

**Table 14.8** Ray Strengths

Ray	Power(dB)
1	0
2	-3
3	-6

**Table 14.9** Parameters of PCS Indoor Model

Environment	Tap Spacing	Number of Taps	Doppler Spectrum	Doppler BW
Residential	50(ns)	2	Gaussian	3Hz
Office	50	4	Gaussian	3
Commercial	50	12	Flat	30

section, uses a symbol time spaced TDL (correlated tap gain functions) to reduce the computational load.

**Discrete Models for PCS Applications** For PCS communication systems operating in the 2-GHz band, the standards bodies have agreed on a set of discrete models for typical operating environments [25]. These models are summarized in Tables 14.7, 14.8, and 14.9. For the model given in Table 14.7, the ray strengths  $E \{ |\tilde{a}|^2 \}$  are given in Table 14.8.

It should be noted again that the differential delays of 50 ns (indoor model) are very small compared to the symbol time of proposed PCS systems. Hence, either the fading should be treated as frequency nonselective, or a bandlimited TDL model with symbol time spacing should be used for simulations.

**Discrete Multipath Channel Models for 3G Wideband CDMA Systems** Cellular communication systems are in their third generation of evolution, and the third generation systems (3G) will use wideband CDMA operating around 2 GHz. Examples of the discrete channel models proposed for 3G systems are shown in Table 14.10 (Case 1: Indoor, Case 2: Indoor or Pedestrian, Case 3: Vehicular) [26].

**Table 14.10** Parameters for 3G Wideband CDMA Channels

Case 1 (3 km/h)		Case 2 (3 km/h)		Case 3 (120 km/h)	
Delay (ns)	Power (dB)	Delay (ns)	Power (dB)	Delay (ns)	Power (dB)
0	0.0	0	0.0	0	0.0
244	-9.6	244	-12.5	244	-2.4
488	-35.5	488	-24.7	488	-6.5
				732	-9.4
				936	-12.7
				1220	-13.3
				1708	-15.4
				1953	-25.4

#### 14.7.4 Models for Indoor Wireless Channels

Fading characteristics of indoor wireless channels are very different from those of vehicular channels due to differences in physical environments (dimensions, materials, etc.) and propagation mechanisms. Outdoor vehicular environments are characterized by larger cells of the order of kilometers and a smaller number of multipath components. Indoor environments, on the other hand, are characterized by smaller dimensions (tens of meters) and a large number of multipath components due to reflections from walls, tables, and other flat work surfaces. There are a number of statistical models for indoor channels derived from measurements and, by and large, the indoor models can be categorized as dense discrete multipath models with an rms delay spread in the range of 30 to 300 ns with each component having Ricean envelope statistics [23]. The path loss index typically varies from 1.8 to 4. Additional details of the indoor channel characteristics may be found in the references [27–31]. The simulation techniques for indoor channels are the same as those we have seen for other multipath channels. However, the small differential delays encountered in indoor situations might require the conversion of nonuniformly spaced TDL models to uniformly spaced models as discussed in Section 14.7.2.

### 14.8 Summary

The overall performance of a communication system is significantly impacted by the distortion, noise, and interference introduced by the communication channels over which they operate. To assess communication system performance, and to design and optimize the signal-processing operations in the transmitter and receiver, we need simulation models for communication channels.

The simplest simulation model for a communication channel is the transfer function model, which can be used for time-invariant communication channels such as optical fibers and electrical cables. Radio communication channels, on the other hand, require more complex models to account for the multipath effect and the time variations (fading) in the channel characteristics, especially in mobile channels.

The simulation model for multipath fading channels has the structural form of a tapped delay line with time-varying tap gains, which are modeled as stationary random processes over observation intervals for which the stationarity assumption applies. For mobile applications, fading in the communication channel is characterized by complex Gaussian processes with appropriate power spectral density functions. Sampled values of tap gain processes in the tapped delay line model are generated by filtering uncorrelated Gaussian sequences with FIR filters which shape the power spectral densities.

For most applications, the tap gains can be assumed to be uncorrelated. However, in some simulation cases, the tap gain processes in the simulation models will be correlated. Generating a set of correlated tap gain processes is, in general, a difficult problem. If the processes involved are Gaussian and have the same power spectral densities, this problem is easily handled.

The literature on measurements of mobile and other radio channels is vast and varied. For simulation purposes we often rely on statistical models derived from measurements. Many examples of the models used for designing and evaluating the performance of second- and third-generation mobile communication systems were presented in this chapter. The reader can find additional models and details in the references.

## 14.9 Further Reading

A vast amount of material has been published on the characterization and modeling of wireless channels and only the most fundamental material is included in this chapter. Almost every issue of the *IEEE Transactions on Wireless Communications*, the *IEEE Transactions on Communications*, and the *IEEE Transactions on Antennas and Propagation* contain new research results in this area. Good collections of papers are given in the double issue of the *IEEE Journal on Selected Areas in Communications* cited below.

- L. J. Greenstein et al., eds., “Channel and Propagation Models for Wireless System Design I and II,” *IEEE Journal on Selected Areas in Communications*, Vol. 20, Nos. 3 and 6, April 2002 and August 2002.

The interested student is also referred to the recent book

- H. L. Bertoni, *Radio Propagation for Modern Wireless Systems*, Upper Saddle River, NJ: Prentice Hall PTR, 2000.

## 14.10 References

1. A. F. Elrefaie, J. K. Townsend, M. B. Romeiser, and K. S. Shanmugan, “Computer Simulation of Digital Lightwave Links,” *IEEE Journal on Selected Areas in Communications*, Vol. 6, No. 1, January 1984, pp. 94–106.

2. D. G. Duff, "Computer-Aided Design of Digital Lightwave Systems," *IEEE Journal on Selected Areas in Communications*, Vol. 2, No. 1, January 1984, pp. 171–185.
3. P. K. Cheo, *Fiber Optic Devices and Systems*, New York: Prentice Hall, 1985.
4. H. Liebe, "Modeling the Attenuation and Phase of Radio Waves in Air at Frequencies Below 1000GHz," *Radio Science*, Vol. 16, No. 6, 1981, pp. 1183–1199.
5. R. K. Crane, "Prediction of Attenuation by Rain," *IEEE Transactions on Communications*, Vol. 28, No. 9, September 1980, pp. 1717–1773.
6. L. J. Ippolito, *Radio Wave Propagation in Satellite Communications*, New York: Van Nostrand, 1986.
7. W. L. Flock, "Propagation Effects in Satellite Communications," NASA Reference 1108, December 1983.
8. L. J. Ippolito et al., "Propagation Effects Handbook for Satellite Systems," NASA Reference 1082, June 1983.
9. P. A. Bello, "Characterization of Randomly Time-Variant Linear Channels," *IEEE Transactions on Communication Systems*, Vol. 11, No. 4, December 1963, pp. 360–393.
10. W. C. Y. Lee, *Mobile Cellular Communications*, New York: McGraw-Hill, 1989.
11. W. C. Jakes, ed., *Microwave Mobile Communications*, New York: Wiley, 1974.
12. B. Glance and L. J. Greenstein, "Frequency Selective Fading Effects in Digital Mobile Radio with Diversity Combining," *IEEE Transactions on Communications*, Vol. 31, No. 9, September 1993, pp. 1085–1094.
13. T. S. Rappaport, *Wireless Communications*, 2nd ed., New York: Prentice Hall, 2002.
14. K. Phalaven and A. H. Leveque, *Mobile Wireless Networks*, New York: Wiley, 1995.
15. B. Sklar, "Rayleigh Fading Channels in Mobile Digital Communications," Parts I and II, *IEEE Communications Magazine*, Vol. 35, July 1997, pp. 90–110.
16. G. D. Durgin, T. S. Rappaport, and D. A. deWolf, "New Analytical Models and Probability Density Functions for Fading in Wireless Communications," *IEEE Transactions on Communications*, Vol. 50, No. 6, June 2002, pp. 1001–1015.

17. S. A. Fetchel and H. Meyer, "A Novel Approach to Modeling and Efficient Simulation of Fading Radio Channel," Proceedings of the International Conference on Communications, Geneva, May 1991, pp. 302–308.
18. W. Escalante, "Simulation of Fading Channels With Arbitrary Scattering Functions," M.S. Thesis, University of Kansas, 1996.
19. V. Fung, T. S. Rappaport, and B. Thoma, "Bit Error Simulation for  $\pi/4$  DQPSK Mobile Radio Communication Using Two-Ray and Measurement-Based Impulse Response Models," *IEEE Journal on Selected Areas in Communications*, Vol. 11, No. 3, April 1993, pp. 393–405.
20. W. D. Rummler, R. P. Counts, and M. Lineger, "Multipath Fading Models for Microwave Digital Radio," *IEEE Communications Magazine*, Vol. 24, No. 11, 1986, pp. 30–42.
21. G. L. Turin et al., "A Statistical Model of Urban Multipath Propagation," *IEEE Transactions on Vehicular Technology*, Vol. 21, February 1972, pp. 1–9.
22. H. Hashemi, "The Indoor Radio Propagation Channel," *Proceedings of the IEEE*, Vol. 81, No. 7, July 1993, pp. 943–968.
23. T. S. Rappaport, S. Y. Seidel, and K. Takamizawa, "Statistical Channel Impulse Response Models for Factory and Open Plan Building Radio Communications System Design," *IEEE Transactions on Communications*, Vol. 39, No. 5, May 1991, pp. 794–806.
24. ETSI, "GSM Recommendations 05.05, Radio Transmission and Reception," Annex 3, 13–16, November, 1988.
25. ANSI J-STD-008, "Personal Station-Base Station Compatibility Requirements for 1.8 to 2.0 GHz CDMA PCS," March 1995.
26. 3GPP Website: A full set of specifications for UMTS release 99 is found on the website [www.3gpp.org](http://www.3gpp.org); [ftp://ftp.3gpp.org/Specs/December\\_99/21\\_series/](ftp://ftp.3gpp.org/Specs/December_99/21_series/).
27. A. A. M. Saleh and R. A. Valenzuela, "A Statistical Model for Indoor Multipath Propagation," *IEEE Journal on Selected Areas in Communication*, Vol. 54, 1987, pp. 128–137.
28. T. S. Rappaport, "Characterization of UHF Multipath Radio Channels in Factory Buildings," *IEEE Transactions on Antennas and Propagation*, Vol. 37, 1989, pp. 1058–1069.
29. R. Ganesh and K. Phalavan, "Statistical Modeling and Computer Simulation of Indoor Radio Channel," *Proceedings of the IEEE*, Vol. 138, 1991, pp. 153–161.
30. J. B. Anderson, T. S. Rappaport, and S. Yoshida, "Propagation Measurements and Models for Wireless Communications," *IEEE Communications Magazine*, Vol. 33, January 1995, pp. 42–49.

31. S. C. Kim, H. L. Bertoni, and M. Stern, "Pulse Propagation Characteristics at 2.4 GHz Inside Buildings," *IEEE Transactions on Vehicular Technology*, Vol. 45, August 1996, pp. 579–592.

## 14.11 Problems

- 14.1 The lowpass transfer function models used for many time-invariant communication channels have a linear tilt in the amplitude response (in dB)

$$|H(f)| = k_1 + k_2 f \quad \text{dB} \quad (14.82)$$

and a quadratic phase response of the form

$$\angle H(f) = g_1 f + g_2 f^2 \quad (14.83)$$

Develop a MATLAB FIR filter model for this transfer function. The tilt in dB/Hz, and the maximum linear and quadratic phase offsets at the band edge are parameters of the model.

- 14.2 In simulating multipath fading channels it is important to calibrate the simulations. It is a common practice to normalize the power profile  $p(\tau)$  and the doppler spectrum  $S(\lambda)$  in order to have unit areas.

- (a) Find the value of  $a$  for normalizing an exponential power profile of the form

$$p(\tau) = a \exp(-a\tau^2) \quad (14.84)$$

- (b) Find the value of  $K$  needed for normalizing the Jakes doppler spectrum.  
 (c) Find the area under the Ricean doppler spectrum defined by (14.61).

- 14.3 Simulate the impact of the linear amplitude tilt and the quadratic phase distortion on a QPSK (LPE) signal with the following parameters: Symbol rate = 1MS/sec, linear tilt = 2dB/MHz, parabolic phase shift =  $\pi/8$  radians at 1Mhz. No transmit filter; receive filter is an ideal integrate and dump detector.

- 14.4 In order to validate the results of simulating the performance of a communication system operating over fading channels, we often compare the performance of the simulated systems against similar systems operating over ideal AWGN channels and/or over a Rayleigh fading channels with ideal phase references. Compare the BER versus  $E_b/N_0$  performance of a QPSK system operating over an AWGN channel with an integrate-and-dump receiver with a differential QPSK system over a Rayleigh fading channel with AWGN. The received signal (bandpass case) is of the form

$$y(t) = R_k \cos(2\pi f_c t + \phi_k + \theta_k) + n(t), \quad kT_s \leq t \leq (k+1)T_s \quad (14.85)$$

where  $T_s$  is the symbol duration,  $n(t)$  represents the AWGN, and  $\phi_k$  represents the differential QPSK modulation. In addition,  $R_k$  and  $\theta_k$  represent the amplitude and phase associated with the Rayleigh fading. Assume that  $R_k$  and  $\theta_k$  change slowly with respect to the symbol rate.

- 14.5 Create a MATLAB simulation model for any two of the GSM models given in Section 14.8. Run BER simulations using the appropriate parameters of the GSM system for vehicle speeds of 25 and 100 MPH. Assume ideal SQRC filtering in the transmitter and receiver and ideal synchronization.
- 14.6 Develop an approach for generating sampled values of a set of correlated Gaussian processes each having a different PSD.
- 14.7 Rerun the MATLAB simulation given in Example 14.1 for different power levels and differential delays and compare the results.
- 14.8 Extend the simulation given in Example 14.1 to a 6-ray model, and run BER simulations for different power profiles as follows (Assume flat fading.)
  - (a) Uniform power over the 6 rays
  - (b) Exponentially decreasing power profile over the 6 taps with the last tap at 10 dB below the first ray

## 14.12 Appendix A: MATLAB Code for Example 14.1

### 14.12.1 Main Program

```

% File: c14_threeray.m
%
% Default parameters
%
NN = 256;                % number of symbols
tb = 0.5;                % bit time
fs = 16;                 % samples/symbol
ebn0db = [1:2:14];      % Eb/N0 vector
%
% Establish QPSK signals
%
x = random_binary(NN,fs)+i*random_binary(NN,fs); % QPSK signal
%
% Input powers and delays
%
p0 = input('Enter P0 > ');
p1 = input('Enter P1 > ');
p2 = input('Enter P2 > ');
delay = input('Enter tau > ');
delay0 = 0; delay1 = 0; delay2 = delay;
%
% Set up the Complex Gaussian (Rayleigh) gains
%
gain1 = sqrt(p1)*abs(randn(1,NN) + i*randn(1,NN));
gain2 = sqrt(p2)*abs(randn(1,NN) + i*randn(1,NN));
for k = 1:NN
    for kk=1:fs
        index=(k-1)*fs+kk;
        ggain1(1,index)=gain1(1,k);
        ggain2(1,index)=gain2(1,k);
    end
end
y1 = x;
for k=1:delay2
    y2(1,k) = y1(1,k)*sqrt(p0);
end
for k=(delay2+1):(NN*fs)
    y2(1,k)= y1(1,k)*sqrt(p0) + ...
    y1(1,k-delay1)*ggain1(1,k)+...
    y1(1,k-delay2)*ggain2(1,k);
end
%

```

```

% Matched filter
%
b = -ones(1,fs); b = b/fs; a = 1;
y = filter(b,a,y2);
%
% End of simulation
%
% Use the semianalytic BER estimator. The following sets
% up the semi analytic estimator. Find the maximum magnitude
% of the cross correlation and the corresponding lag.
%
[cor lags] = vxcorr(x,y);
cmax = max(max(abs(cor)));
nmax = find(abs(cor)==cmax);
timelag = lags(nmax);
corrmag = cmax;
theta = angle(cor(nmax))
y = y*exp(-i*theta); % derotate
%
% Noise BW calibration
%
hh = impz(b,a); ts = 1/16; nbw = (fs/2)*sum(hh.^2);
%
% Delay the input, and do BER estimation on the last 128 bits.
% Use middle sample. Make sure the index does not exceed number
% of input points. Eb should be computed at the receiver input.
%
index = (10*fs+8:fs:(NN-10)*fs+8);
xx = x(index);
yy = y(index-timelag+1);
[n1 n2] = size(y2); ny2=n1*n2;
eb = tb*sum(sum(abs(y2).^2))/ny2;
eb = eb/2;
[peideal,pesystem] = qpsk_berest(xx,yy,ebn0db,eb,tb,nbw);
figure
semilogy(ebn0db,peideal,'b*-',ebn0db,pesystem,'r+-')
xlabel('E_b/N_0 (dB)'); ylabel('Probability of Error'); grid
axis([0 14 10^(-10) 1])
% End of script file.

```

### 14.12.2 Supporting Functions

A number of the supporting functions for this example appeared previously and are not given here. These are:

`qpsk_berest.m` Given in Chapter 10, Appendix C.

`vxcorr.m` Given in Chapter 10, Appendix B.

`random_binary.m` Given in Chapter 10, Appendix A.

## 14.13 Appendix B: MATLAB Code for Example 14.2

### 14.13.1 Main Program

```

% File: c14_Jakes.m
% This program builds up a two-tap TDL model and computes the output
% for the two inpput signal of interest.
% Generate tapweights
%
fd = 100; impw = jakes_filter(fd);
%
% Generate tap input processes and Run through doppler filter.
%
x1 = randn(1,256)+i*randn(1,256); y1 = filter(impw,1,x1);
x2 = randn(1,256)+i*randn(1,256); y2 = filter(impw,1,x2);
%
% Discard the first 128 points since the FIR filter transient
% Scale them for power and Interpolate weight values
% Interpolation factor =100 for the QPSK sampling rate of 160000/sec;
%
z1(1:128) = y1(129:256); z2(1:128) = y2(129:256);
z2 = sqrt(0.5)*z2; m = 100;
tw1 = linear_interp(z1,m); tw2 = linear_interp(z2,m);
%
% Generate QPSK signal and filter it.
%
nbits = 512; nsamples = 16; ntotal = 8192;
qpsk_sig = random_binary(nbits,nsamples)+i*random_binary...
    (nbits,nsamples);
%
%Generate output of tap1 (size the vectors first).
%
input1 = qpsk_sig(1:8184); output1 = tw1(1:8184).*input1;
%
% Delay the input by eight samples (this is the delay specified
% in term of number of samples at the sampling rate of
% 16,000 samples/sec and generate the output of tap 2.
%
input2 = qpsk_sig(9:8192); output2 = tw2(9:8192).*input2;
%
% Add the two outptus and genrate overall output.
%
qpsk_output = output1+output2;
%
% Generate the 1000 Hz complex exponential and run it through the TDL
% model. This could be done at the higher sampling rate of 16,0000

```

```

% samples per sec or at a lower rate. At the lower rate the tap
% spacing must be recomputed in number of samples at the lower rate.
% Also the interpolation of the tap gain functions must now be at
% the lower rate. In this example we will use the higher sampling rate.
%
ts = 1/160000; time = (ts:ts:8200*ts);
cexp = exp(2*pi*i*1000*time);
input1 = cexp(1:8184); output3 = tw1(1:8184).*input1;
input2 = cexp(9:8192); output4 = tw2(9:8192).*input2;
%
% Add the two outputs and generate overall output.
%
cexp_out = output3+output4;
[psdcexp,freq,ptotal,pmax] = linear_psd(cexp(1:8184),8184,ts);
[psdcexp_out,freq,ptotal,pmax] = linear_psd(cexp_out(1:8184),8184,ts);
%
subplot(2,1,1)
plot(freq(4100:4180), psdcexp(4100:4180)); grid;
xlabel('Frequency (Hz)'); ylabel('PSD')
subplot(2,1,2)
plot(freq(4100:4180), psdcexp_out(4100:4180),'r'); grid;
xlabel('Frequency (Hz)'); ylabel('PSD')
figure; subplot(2,1,1)
plot(real(qpsk_sig(501:1000)),'r'); grid;
xlabel('Sample Index'); ylabel('Direct Input');
axis([0 500 -2 2])
subplot(2,1,2)
plot(real(qpsk_output(501:1000)));grid;
xlabel('Sample Index'); ylabel('Direct Output');
figure;
plot(abs(output3(3000:6000))); grid
xlabel('Sample Index'); ylabel('Envelope Magnitude')
% End script file.

```

### 14.13.2 Supporting Functions

#### jakes\_filter.m

```

% File: Jakes_filter.m
function [impw] = jakes_filter(fd)
% FIR implementation of the Jakes filter (128 points)
n = 512; nn = 2*n; % nn is FFT block size
fs = 0:fd/64:fd; % sampling frequency = 16*fd
H = zeros(1,n); % initialize H(f)
for k=1:(n/8+1) % psd for k=1:65
    jpsd(k)=1/((1-((fs(k))/fd)^2)^0.5);

```

```

    if(jpsd(k)) > 1000
        jpsd(k)=1000;
    end
    H(k)=jpsd(k)^0.5; % first 65 points of H
end
for k=1:n                % generate negative frequencies
    H(n+k) = H(n+1-k);
end
[inv,time] = linear_fft(H,mn,fd/64); % inverse FFT
imp = real(inv(450:577)); % middle 128 points
impw = imp.*hanning(128)'; % apply hanning window
energy = sum(impw.^2); % compute energy
impw = impw/(energy^0.5); % normalize
% End of function file.

```

### **linear\_psd.m**

```

% File: linear_psd.m
function [psd,freq,ptotal,pmax] = linear_psd(x,n,ts)
% This function takes the n time domain samples (real or complex)
% and finds the psd by taking (fft/n)^2. The two sided spectrum is
% produced by shifting the psd.
% NOTE: n must be an even number, preferably a power of 2.
for k=1:n
    y(k) = 0.;
end
for k=1:n
    freq (k) =( k-1-(n/2))/(n*ts);
    y(k) = x(k)*((-1.0)^k);
end;
v = fft(y)/n; psd = abs (v).^2;
pmax = max(psd); ptotal = sum(psd)
% End of function file.

```